

# An XMM-Newton spectral survey of 12 micron selected galaxies. II. Implications for AGN selection and unification

Murray Brightman<sup>2,1\*</sup> and Kirpal Nandra<sup>2,1</sup>

<sup>1</sup>*Astrophysics Group, Imperial College London, Blackett Laboratory, Prince Consort Road, London SW7 2AW*

<sup>2</sup>*Max-Planck-Institut für extraterrestrische Physik, Giessenbachstrasse 1, D-85748, Garching bei München, Germany*

Accepted 0000 December 00. Received 0000 December 00; in original form 0000 October 00

## ABSTRACT

We present a multi-waveband analysis of a 126 galaxy sub-sample of the 12 micron galaxy sample (12MGS), for which we have carried out a detailed X-ray spectral analysis of in a previous paper. We determine the activity class of the galaxies by way of optical line ratio diagnostics and we characterise the optical classes by their X-ray, 12  $\mu\text{m}$  and [O III] luminosities and by their X-ray spectral properties. Our most interesting results from this investigation are as follows: (i) Seyfert (Sy) 1s and Sy 2s show a significantly different X-ray luminosity distributions from each other (ii) Sy 2 galaxies with a detection of an HBLR show a significantly higher X-ray luminosity than those without a detection, supporting the findings of Tran (2003) (iii) Sy 1s also present a significantly different 12  $\mu\text{m}$  luminosity distribution from both intermediate Sy types and Sy 2s (iv) the Seyfert 2 fraction decreases towards high X-ray luminosities (v) X-ray indications of AGN power agree well with the optical classifications (vi) There is X-ray evidence for the presence of an AGN in 17% of H II/AGN composite galaxies and 40% of LINERs (vii) we advocate the use of a 2–10 keV X-ray luminosity of  $10^{41} \text{ erg s}^{-1}$  in the X-ray selection of AGN, rather than  $10^{42} \text{ erg s}^{-1}$ , which we find gives a contamination rate of only 3% from star-forming galaxies. (viii) from an analysis of the X-ray power-law index,  $\Gamma$ , we find that Sy 1s and Sy 2 have the same intrinsic distributions, implying that the central engines are the same, in support of AGN unification schemes (ix) in 24% of cases the absorption measured in the X-ray spectra does not correspond directly with that implied in the optical band from the visibility of the broad line regions (BLRs), which is in conflict with AGN unification schemes (x) We confirm previous work showing that the obscured fraction in AGN declines at high X-ray luminosity, but also find a decrease at low luminosity having peaked at  $L_X \sim 10^{42} \text{ erg s}^{-1}$ , suggesting that source luminosity has a large effect on the obscuring material, therefore also calling for a modification to unified schemes (xi) The average obscured and Compton thick fractions for this sample are  $62 \pm 5\%$  and  $20 \pm 4\%$  respectively, which are higher than hard X-ray and optically selected samples, therefore supporting mid-infrared (MIR) selection as a relatively unbiased method of selecting AGN (xii) we assess the use of the ‘T’ ratio ( $F_X/F_{[\text{O III}]}$ ) for selecting Compton thick candidates. We conclude here that this quantity can often be unreliable due to uncertainties in the extinction corrections to the [O III] flux. These results have important impacts on AGN selection and unification and the results from the 12MGS are particularly useful as a local analogue to *Spitzer*/MIPS 24  $\mu\text{m}$  samples selected at  $z=1$ , as observed 24  $\mu\text{m}$  emission originates at rest-frame 12  $\mu\text{m}$  in sources at this redshift.

**Key words:** galaxies: active - galaxies: Seyfert - X-rays: galaxies

## 1 INTRODUCTION

There are currently ongoing debates in astrophysics concerning many aspects of nuclear activity in galaxies. It has

\* E-mail: mbright@mpe.mpg.de

become widely accepted though, that most massive galaxies harbour a super-massive black hole in their nuclei (Kormendy 1988; Magorrian et al. 1998), and that this component is central to the growth and evolution of the host galaxy itself (eg. Ferrarese & Merritt 2000; Gebhardt et al. 2000). It is believed that accretion of matter onto these black holes is the energy source for what we know as active galactic nuclei (AGN). The term ‘active’ when applied to the nucleus of a galaxy is historically quite general and describes a nucleus which displays characteristics which cannot be attributed to normal stellar processes. This can be highly wavelength dependent and as such, the identification of AGN depends on the wavelength regime used. A prime example is NGC 6240, which was identified as an AGN from its X-ray luminosity, which exceeds any X-ray luminosity observed from pure star-forming galaxies (Schulz et al. 1998), but does not appear as an AGN in the optical. These types of AGN, which do not show themselves at all wavelengths, can be called ‘hidden’ AGN. AGN activity continues to be uncovered in previously thought of normal galaxies, such as with the use of MIR high excitation lines (e.g. Goulding & Alexander 2009) or high spatial resolution X-ray imaging (e.g. Grier et al. 2010). It is thus important to investigate the identification technique which selects AGN most completely.

AGN also appear in many different types, ranging from low ionisation nuclear emission-line regions (LINERs, Heckman 1980) to quasars, and attempts have been made to unify these types into a single scheme. The most successful unification scheme explains the difference between the different Seyfert types by the orientation of the observer with respect to a circumnuclear structure of dust, now commonly believed to be a torus (Antonucci 1993; Urry & Padovani 1995). This scheme has held up well, owing to its simplicity, but has come under increasing pressure of late. For example, there is increasing evidence and supporting theoretical work to suggest that at low luminosity and/or accretion rate, AGN appear differently from their higher luminosity counterparts (e.g. Laor 2003; Nicastro et al. 2003; Tran 2003; Elitzur & Shlosman 2006; Hopkins et al. 2009). LINERs may also be accounted for in part by these low luminosity AGN models, but a consensus on the power generation mechanism in LINERs has not yet been achieved. Obscuration in AGN may also be dependent on luminosity, as has been found in several studies at high luminosity (e.g. Ueda et al. 2003), but also suggested at low luminosity (Akylas & Georgantopoulos 2009; Zhang et al. 2009; Burlon et al. 2010). This has important consequences for the current AGN unification paradigm, which attributes the sole difference between different AGN types to the orientation with respect to the observer.

To investigate the issues of AGN selection and unification, large, statistically complete galaxy samples are required. Most of these are based on flux limited surveys, for example the Revised Shapley-Ames Catalogue of Bright Galaxies (RSA, Sandage et al. 1979) or the CfA sample (Huchra & Burg 1992), both selected in the optical. Optical selection, however, is largely affected by extinction, presenting a bias against reddened sources. Galaxy samples selected at wavelengths less affected by extinction are thus optimal. Hard X-ray ( $>10$  keV) surveys are ideal for avoiding biases against obscuration as at these wavelengths only the heaviest obscuration attenuates them. Current sensitiv-

ity at these wavelengths provided by the *Swift*/BAT and *INTEGRAL* surveys produces samples of sources down to  $L_{\text{HX}} \sim 10^{41}$  erg s $^{-1}$  (e.g. Tueller et al. 2008; Beckmann et al. 2009; Tueller et al. 2010; Cusumano et al. 2010), and thus do not contain the lowest luminosity systems.

An alternative wavelength for AGN selection is the MIR, where the primary radiation of the AGN is re-emitted after having been reprocessed by hot dust. The extended *IRAS* 12 micron galaxy sample (12MGS - Rush, Malkan & Spinoglio 1993, RMS) is a sample of 893 MIR selected local galaxies which contains a high fraction of AGN (13% at the time of publication, RMS). The sample is taken from the *IRAS Faint Source Catalogue, version 2 (FSC-2)* and imposes a flux limit of 0.22 Jy, including only sources with a rising flux density from 12 to 60 microns (to exclude stars) and with a galactic latitude of  $|b| \geq 25$  deg. Being selected in the mid-infrared (MIR) this sample is also relatively unbiased against absorption, low luminosity systems and ‘hidden AGN’. Spinoglio & Malkan (1989) showed that a wide variety of AGN types emit a constant fraction of their bolometric luminosities at this wavelength, and furthermore shown to be true for star forming galaxies as well by Spinoglio et al. (1995). The 12MGS should therefore also be representative of the true number of different active galaxy types in relation to each other and thus ideal for population statistics.

Empirically, 12 micron selection appears to be relatively unbiased with respect to extinction. However, it is expected theoretically that 12  $\mu$ m emission is suppressed in heavily obscured AGN. In the radiation transfer models of Pier & Krolik (1992), the authors investigate the infrared emission of centrally illuminated smooth dust tori, thought to exist in AGN. A main conclusion of this is that these dust tori do not emit isotropically in the mid-IR, and that emission in the ‘face-on’ direction is greater than that in the ‘edge-on’ direction. This has important consequences for our work, as it would suggest that 12  $\mu$ m selection is biased against these edge on systems. Alternatively, much support has been gained recently for a ‘clumpy’ torus in AGN, where the dust distribution is not smooth, but instead made up of individual clouds (e.g. Ramos Almeida et al. 2009; Hönig et al. 2010; Mullaney et al. 2011). Nenkova et al. (2008) present a model describing the infra-red emission of such a torus and find that at 12  $\mu$ m, and at all IR wavelengths, the torus emission is isotropic, in contrast to the smooth torus models. A key observational test of this would be the ratio of the X-ray to mid-IR fluxes, which should be higher for heavily absorbed systems in smooth torus distributions, when absorption in the X-ray band has been accounted for, due to the higher mid-IR emission in the face-on systems. The models of Pier & Krolik (1992) predict an order of magnitude difference in the 12  $\mu$ m flux for an increase in the  $N_{\text{H}}$  from  $\sim 10^{23}$  to  $\sim 10^{24}$  for a torus seen edge on. Horst et al. (2008), however, show that Seyfert 1s, Seyfert 2 and even Compton thick AGN show the same tight correlation between their X-ray and mid-IR fluxes, which supports the clumpy torus model over the smooth one. They also rule out any contamination of the mid-IR flux from the host galaxy by using high resolution, adaptive optics assisted, 12.3  $\mu$ m imaging, isolating the torus spatially. These results are in support of 12  $\mu$ m being a relatively unbiased selection method for AGN.

In this paper, we aim to broadly investigate the nuclear activity in local ( $z < 0.1$ ) galaxies, using the 12MGS

as a relatively unbiased and representative parent sample. We base this investigation on a sub-sample of 126 galaxies in the 12MGS which we presented in a previous publication (Brightman & Nandra 2010, paper I hereafter). This sub-sample consists of all galaxies in the 12MGS for which an *XMM-Newton* observation was available as of December 2008 (which included serendipitous observations of NGC 0214, 4559 and 7771), and for which the X-ray spectrum could be at least fitted with the most basic spectral model. For more details regarding the X-ray observations and spectral analysis, the reader is referred to paper I. In paper I, we presented a detailed X-ray spectral analysis of these galaxies, assessing the intrinsic luminosity,  $L_X$ , the photon index,  $\Gamma$  and the line of sight absorption,  $N_H$ , which are key parameters for our investigation here. We start in Section 2 where we uniformly classify the activity type in our sample using optical emission line data from the literature and BPT (Baldwin, Phillips & Terlevich 1981) diagnostics. Secondly in Section 3 we characterise the different optical types in 2-10 keV, 12  $\mu$ m and [O III] luminosities and in Section 4 we investigate the X-ray properties of these types, including the continuum slope,  $\Gamma$  and the obscuration,  $N_H$ . Finally in Section 5 we investigate the relationship between the X-ray and MIR emission in this sample. We discuss these results within the context of AGN selection and unification in Section 6 and present our conclusions in Section 7.

## 2 OPTICAL EMISSION LINE ACTIVITY CLASSIFICATION

In paper I we used an observed 2-10 keV X-ray luminosity of  $10^{42}$  erg s $^{-1}$  to identify unambiguous AGN activity in our sample. This method is clearly very crude as it will miss all low luminosity AGN. The classical method of defining activity type is via so called BPT diagrams which use the ratios of optical emission lines to determine the dominant source of ionising radiation of emission line galaxies, be it photo-ionisation by stars, by a harder non-thermal source such as an AGN or by collisional excitation by shocks, as may be the case in LINERs. Here we apply such a scheme in order to investigate the X-ray properties of the various optical types.

We use the scheme of Kewley et al. (2006) to classify the galaxies in our sample from optical narrow line emission (Fig. 1). This scheme uses theoretical ‘maximal starburst’ lines from Kewley et al. (2001) which are derived from stellar population and photoionisation models and define the limit of ‘pure’ stellar photoionisation. Any sources which lie above these lines are likely to be photoionized by another source of ionization such as an AGN or shocks. This scheme relies on three diagrams, diagram (1) using [O III]/H $\beta$  vs. [N II]/H $\alpha$ , diagram (2) using [O III]/H $\beta$  vs. [S II]/H $\alpha$  and diagram (3) using [O III]/H $\beta$  vs. [O I]/H $\alpha$ . They also define a region of composite ‘starburst/AGN’ activity on diagram 1, which lies below the theoretical starburst limit, but above an empirically defined pure-starburst limit (Kauffmann et al. 2003). They argue that since the [N II]/H $\alpha$  ratio is most sensitive to the presence of an AGN due to the ratio ‘saturating’ at high metallicities, which exist in extreme H II galaxies, any source beyond the pure starburst limit must contain an AGN. On diagrams 2 and 3, they derive new empirical separation lines

between Seyfert 2s and LINERs using high signal-to-noise SDSS data, which show distinct branches on these diagrams, belonging to these emission line galaxy types.

We have obtained narrow line ratios from a compilation of unpublished data from Rodriguez et al. (in preparation) for 70 of the galaxies in our sample of 126 sources. For the rest, where they exist, we have compiled from the literature the [O III]/H $\beta$ , [O I]/H $\alpha$ , [N II]/H $\alpha$  and [S II]/H $\alpha$  line ratios which are needed for this classification method. In five cases we have used SDSS DR7 emission line data, where no literature line ratio data exists. These data originate from the SPECBS code which extracts emission line data from the SPECTRO2D pipeline reduced spectra<sup>1</sup> done at Princeton University. Table 1 presents these data, including the reference for the line ratio data. Fig. 1 presents the BPT classifications diagrammatically.

We adopt a classification based on the three diagrams. In the cases where the classification differs on one or two diagrams for the same galaxy, we use a composite classification such as ‘H II/AGN’, ‘Sy2/LINER’ or ‘H II/LINER’. If the classification differs between diagram 2 and diagram 3, we choose the classification given by diagram 3, as [S II]/H $\alpha$  is said to be the least effective diagnostic in activity classification and [O I]/H $\alpha$  is most sensitive to shocks, making it better at identifying LINERs (Kewley et al. 2001). Each diagram requires 4 emission lines for the classification. If data for all 4 lines are not available, we cannot use that diagram for the classification.

Finally we supersede this activity classification, which is based on narrow line diagnostics, if a classification of a Seyfert 1-1.9 has been given in the literature. The classification of these sources based on the detection of broad lines is dependent on the methods used by each author, and thus differing classifications can be given for one source. It is also possible that a source changes classification. We have attempted to be as uniform as possible with our literature choice, taking the majority of the broad line classifications from Rodriguez, et al (25/33), and de Grijs et al. (1992) (4/33).

The results of this classification are also presented in Table 1. Our sample then consists of 12 Seyfert 1 galaxies, 16 Seyfert 1.2-1.5 galaxies, 5 Seyfert 1.8-1.9 galaxies (21 Seyfert 1.2-1.9 galaxies), 37 Seyfert 2 galaxies, 11 LINERs, 2 ambiguous Seyfert 2/LINERs, 13 H II galaxies, 18 H II/AGN composites, 3 ambiguous H II/LINERs, and 9 galaxies which remain unclassified due to insufficient optical emission line data existing in the literature.

The 12MGS as published by RMS contained 893 galaxies. At the time of publication these included 53 Seyfert 1s, 63 Seyfert 2s, 29 LINERs and 38 star forming galaxies, whereas the rest of the sample were called normal galaxies. Table 3 lists the proportions of the various optical types in the complete 12MGS and in our *XMM-Newton* sub-sample in percentage form with their binomial errors. The ratio of Seyfert 2s to Seyfert 1 in the original sample was 1.19. If we group Seyfert 1, 1.2 and 1.5s together as Seyfert 1s and Seyfert 1.8, 1.9 and 2s together as Seyfert 2s as is commonly done, we have a ratio of 1.5 in our sub-sample. We also note, however, a ratio of 1.12 narrow line (Sy 2) to broad line (Sy

<sup>1</sup> <http://www.sdss.org/dr7/products/spectra/index.html>

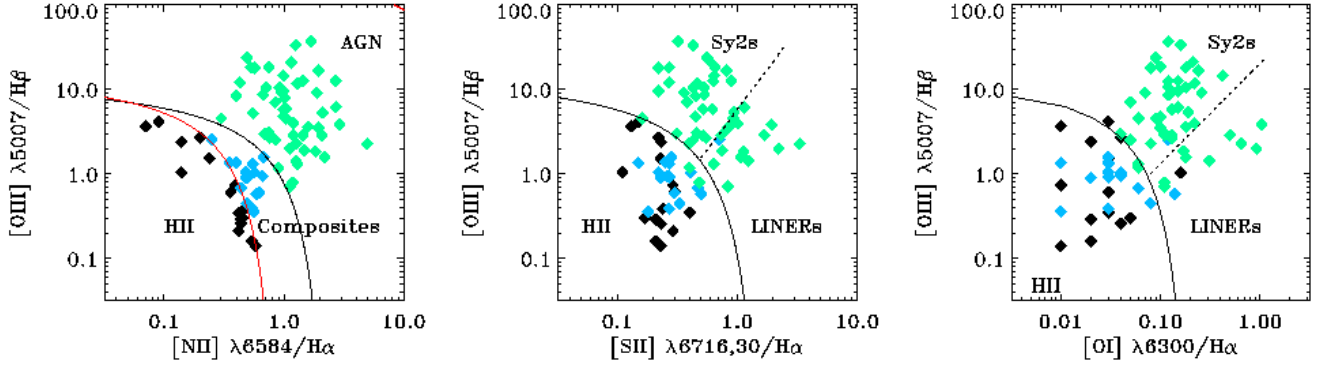


**Figure 1.** BPT diagrams showing diagram (1) on the left using  $[O\text{ III}]\lambda 5007/H\beta$  vs.  $[N\text{ II}]\lambda 6584/H\alpha$ , diagram (2) in the middle using  $[O\text{ III}]\lambda 5007/H\beta$  vs.  $[S\text{ II}]\lambda 6716,30/H\alpha$  and diagram (3) on the right using  $[O\text{ III}]\lambda 5007/H\beta$  vs.  $[O\text{ I}]\lambda 8300/H\alpha$ . H II galaxies (black), Seyfert 2s (blue) and LINERs (green) are separated using the classification scheme of Kewley et al. (2006). Diagram 1 identifies pure H II galaxies (black), H II/AGN composites (light blue) and pure AGN (turquoise), but does not distinguish between Sy 2s and LINERs. We plot the types classified in diagram 1 on the following two diagrams to display the agreement between the two.

1-1.9) in our sample. The ratio of LINERs to Seyfert galaxies in the original sample is 0.25, whereas our sample contains 0.14 LINERs to Seyferts. And finally, the ratio of star-forming galaxies to Seyferts in the original sample was 0.33, whereas our sample contains 0.44 when H II/AGN composite galaxies are included, or 0.19 when only pure star-forming galaxies are counted. We show here that the *XMM-Newton* subsample we use is thus representative of the complete 12MGS as published by RMS, and not biased towards AGN. We do note however, that since RMS, optical type proportions have changed, for example, by the discovery of many Seyfert 2 galaxies in normal/star-forming galaxies (eg. Dopita et al. 1998; Thean et al. 2001). Furthermore, the 12MGS is not spectroscopically complete (Hunt & Malkan 1999), so there may yet be undiscovered active galaxies within the normal galaxy population. However, the majority of sources not spectroscopically identified are southern galaxies, so we posit that the incompleteness is not caused by a bias against faint sources, rather by observability. The classification of the entire sample has not been done uniformly with a single classification scheme, but this will be the subject of future work by Rodriguez et al. (in preparation). In this study, we benefit from a uniform classification of all the galaxies in our sub-sample, which is almost spectroscopically complete.

In addition to the optical line ratios used for diagnostics, we also gather  $[O\text{ III}]\lambda 5007$  line fluxes, which are often used as an indicator of the intrinsic luminosity of the central engine. We apply reddening corrections to these fluxes using the method described by Veilleux & Osterbrock (1987) which makes use of the observed Balmer decrement,  $H\alpha/H\beta$  and assumes an intrinsic value of  $H\alpha/H\beta=2.85$  for H II like galaxies, and  $H\alpha/H\beta=3.1$  for AGN. For Balmer decrements less than the assumed intrinsic value, we do not apply the reddening correction. These data are also presented in Table 1.

Having used optical emission line diagnostics to classify the galaxies in this sample, we can then define a set of AGN within the sample based on optical data. We call any galaxy with a Seyfert classification an AGN, of which there are 70 in our sample. If a hidden BLR (HBLR) has been detected, either using near-IR spectroscopy, or optical

**Table 3.** Proportion of optical types in our *XMM-Newton* subsample compared with the proportions from the entire 12MGS (RMS, Rush, Malkan & Spinoglio 1993) with binomial errors. ‘all galaxies’ refers to all 893 members of the 12MGS, ‘active galaxies’ refers to all Seyferts, LINERs and H II galaxies and ‘comp’ refers to H II/AGN composites.

Proportion	12MGS (RMS)	<i>XMM-Newton</i> sub-sample
Sy/all galaxies	$13 \pm 1.1\%$	-
Sy/active galaxies	$63 \pm 3.1\%$	$56 \pm 4.4\%$
Sy 1.8-2/Sy	$54 \pm 4.6\%$	$60 \pm 5.9\%$
Sy 2/Sy	-	$53 \pm 5.9\%$
LINER/(LINER+Sy)	$20 \pm 3.3\%$	$14 \pm 3.9\%$
H II/(H II+Sy)	$25 \pm 3.5\%$	$16 \pm 4.0\%$
(H II+comp)/(H II+comp+Sy)	-	$31 \pm 4.6\%$

spectropolarimetry, we classify this as an AGN, regardless of the classification based on non-polarimetric optical spectroscopy. Eight objects without a Seyfert classification, but with an HBLR are in our sample. We obtain this information from Véron-Cetty & Véron (2006), who present a compilation of HBLR data which has been compiled from the literature for their catalogue of AGN, which we give in Table 2. Table 2 also lists all mulitwavelength data used in the analysis of this paper.

### 3 LUMINOSITY CHARACTERISTICS OF THE 12MGS

Following the optical emission line activity classification we have conducted for our sub-sample, we go on to investigate the luminosity characteristics of the different optical types. Table 4 presents the mean luminosities of each optical type including the standard deviation of the distribution. Plotted in Fig. 2 are histograms of the luminosity distributions for pure H II galaxies and H II/AGN composites, Seyfert 1s and intermediate Seyfert 1.2-1.9s and Seyfert 2s and LINERs at

2-10 keV (intrinsic), 12  $\mu\text{m}$  and the [O III] line. We exclude 3C273 in our luminosity analysis due to its blazar nature.

In X-rays, it would appear that H II/AGN composite galaxies, thought to harbour at least a low level AGN, have very similar luminosity distributions to pure H II galaxies. Strict Seyfert 1s have a greater average luminosity than the intermediate types and Seyfert 2s and these in turn have a greater average luminosity than LINERs. A Kolmogorov-Smirnov (K-S) test shows a significant difference between Seyfert 1s and Seyfert 2s at the 99.4% confidence level, but does not show a significant difference for other associated pairs at the greater than 99% confidence level. The X-ray luminosities are absorption corrected, and thus, the difference seen between the Seyfert 2s and Seyfert 1s must be intrinsic, rather than due to obscuration.

At 12  $\mu\text{m}$ , H II galaxies and H II/AGN composites have the same average luminosity. Strict Seyfert 1s however, show a much larger average 12  $\mu\text{m}$  luminosity than the intermediate type Seyferts and Seyfert 2s. Seyfert 2s again have a greater average luminosity than LINERs. A K-S test shows that Seyfert 1s are distinctly different from both Seyfert 1.2-1.9s and Seyfert 2s at the 99.99% confidence level.

Finally, for extinction corrected [O III] luminosities, we find a greater average luminosity for H II/AGN composites when compared to pure H II galaxies. Seyfert 1s have on average almost a two orders of magnitude greater [O III] luminosity than the intermediate Seyferts and Seyfert 2s. Again, we find a greater average luminosity for Seyfert 2s when compared to LINERs, though this may be expected as Seyfert 2s and LINERs are split using the [O III]/H $\beta$  line ratio. A K-S test, however, only shows Seyfert 2s and LINERs to be belonging to different populations at the 99% confidence level. Furthermore, we note that for  $L_{[\text{O III}]} > 10^{42} \text{ erg s}^{-1}$  there are no pure star forming galaxies. Although selecting AGN above this luminosity would yield sources 100 times more luminous than X-ray selection at  $10^{42} \text{ erg s}^{-1}$ , it is still useful to know for sources where standard BPT diagnostics are not possible due to H $\alpha$  having been redshifted out of the optical band and/or X-ray data are not available. In this case the [O III]/H $\beta$  ratio would still be available for AGN/LINER separation.

At all three wavelengths, after accounting for reddening/absorption, Seyfert 1s are intrinsically more luminous than Seyfert 2s. This has been found similarly in the *Swift*/BAT hard X-ray sample by Winter et al. (2010) for [O III] and 2-10 keV luminosities.

We also investigate the distribution of luminosities for Seyfert 2s with a detection of an HBLR (either in optical spectropolarimetry, or near-IR spectroscopy) and without a detection. The mean luminosities of the Seyfert 2s with an HBLR detection is over an order of magnitude higher in X-rays than those without a detection, and a K-S test shows that these distributions are significantly different at the 99.7% confidence level. Fig. 3 plots these X-ray luminosity distributions along with the Seyfert 1-1.9 X-ray luminosity distribution for comparison. This results was originally presented by Tran (2003), also working on the 12MGS.

Further to the luminosity distributions of these optical types, we also investigate optical type fractions as functions of luminosity. These are presented in Fig. 4 which shows the Seyfert type 2 fraction of all Seyferts, the Seyfert intermediate type fraction of all type 1 Seyferts and the LINER

**Table 4.** Mean luminosities of the different optical types at 2-10 keV (intrinsic), 12  $\mu\text{m}$  and the [O III] line, with their standard deviations,  $\sigma$ .

Type	$L_X$	$\sigma$	$L_{12}$ log <sub>10</sub>	$\sigma$ erg s <sup>-1</sup>	$L_{\text{OIII}}$	$\sigma$
Sy 1	43.34	0.72	44.75	0.64	43.00	1.07
Sy 1.2-1.9	42.60	1.32	43.44	0.79	41.17	1.24
Sy 2	41.97	1.29	43.68	0.63	41.23	1.27
LINERs	40.80	1.63	42.87	0.90	39.26	1.82
H II	40.00	0.93	43.33	0.89	39.30	1.29
H II/AGN	40.51	1.42	43.47	1.07	40.41	1.51
Sy 2 (HBLR)	42.83	0.78	44.01	0.67	41.83	0.90
Sy 2 (non-HBLR)	41.51	1.27	43.50	0.54	40.91	1.34

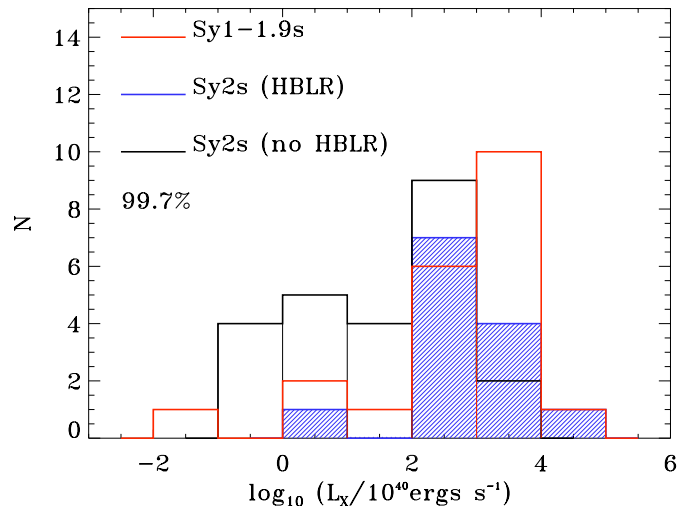


**Figure 3.** X-ray luminosity distribution of Seyferts 2s with detected HBLRs (blue with hatching), Seyfert 2s with no HBLR detected (black) and Seyfert 1-1.9s (red).

fraction of all Seyfert and LINER galaxies against 12  $\mu\text{m}$  and intrinsic X-ray luminosity. The vertical error bars we plot here are 68% confidence intervals calculated using a Bayesian based method presented in Cameron (2010) which is particularly useful for fractions at or close to 1 or 0. For cases where the fractions are 1 or 0, we plot only the confidence interval, marked by a grey bar. We find here that the Seyfert type 2 fraction is a strong decreasing function of X-ray luminosity, dropping significantly from  $\sim 60\%$  to  $\sim 30\%$  above  $10^{43} \text{ erg s}^{-1}$ . A weaker and less significant decline is also seen with 12  $\mu\text{m}$  luminosity. We do find however that the fraction of intermediate Seyfert types of all type 1 Seyferts is a strong decreasing function of 12  $\mu\text{m}$  luminosity, though this is not evident in X-ray luminosity. The LINER fraction declines with both 12  $\mu\text{m}$  and X-ray luminosities.

#### 4 X-RAY PROPERTIES OF THE 12MGS

We now explore the X-ray properties of our sub-sample according to optical type, building on the analysis in paper I.

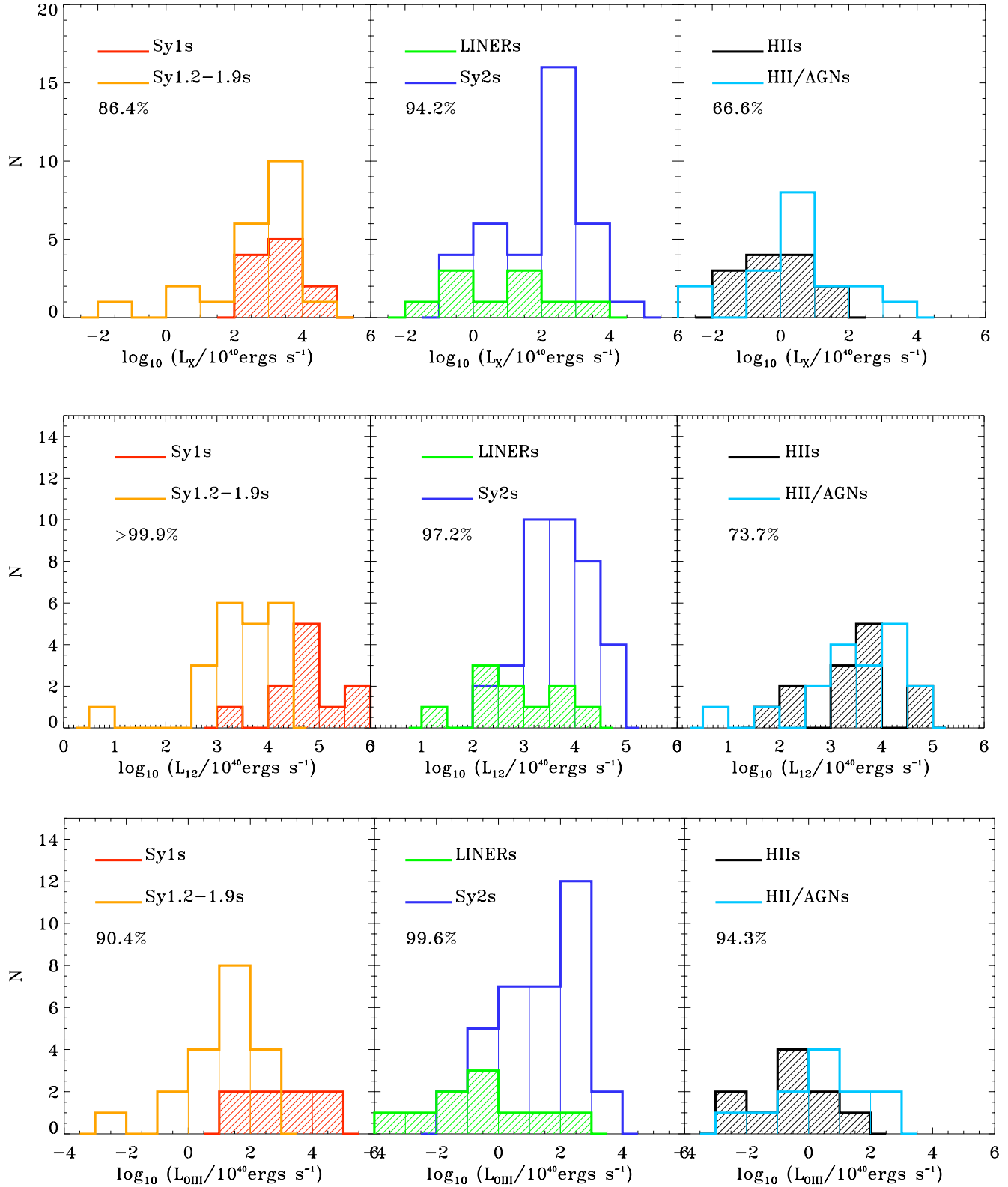


**Figure 2.** Luminosity distribution of the sources by optical type. Left panels - Seyfert 1s (red) and Seyfert 1.2-1.9 galaxies (yellow). Middle panels - Seyfert 2 galaxies (blue) and LINERs (green). Right panels - H II galaxies (black) and H II/AGN composites (light blue). Top panels - intrinsic 2-10 keV luminosity. Middle panels - 12  $\mu\text{m}$  luminosity. Bottom panel - [O III] (corrected) luminosity.

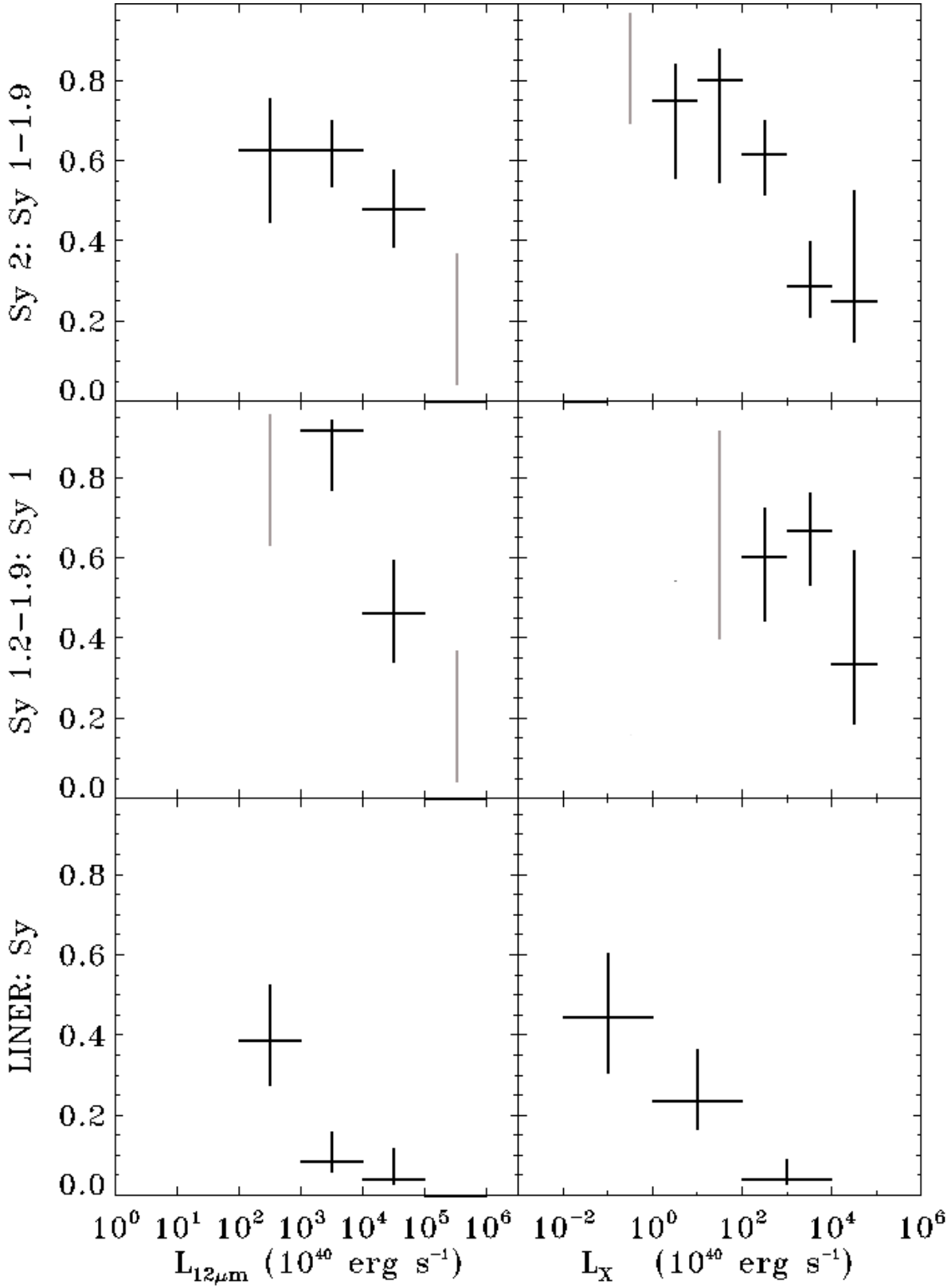


**Figure 4.** Optical type fractions versus 12  $\mu\text{m}$  luminosity and intrinsic 2-10 keV X-ray luminosity with 68% confidence intervals plotted as vertical error bars. Lone grey vertical bars represent confidence intervals on the fraction where the computed fraction is 1 or 0 (described in text). Top - Seyfert type 2 fraction of all Seyferts; middle - intermediate Seyfert (type 1.2-1.9) fraction of all type 1 Seyferts; bottom - LINER fraction of all Seyfert and LINERs galaxies.

There are 78/126 (=62%) galaxies defined as AGN in our sample using our optical definitions, compared to 60/126 (=48%) using an observed 2-10 keV X-ray luminosity of  $10^{42}$  ergs $^{-1}$  as a discriminator. In general we find good agreement between the unambiguous X-ray AGN we found in paper I and the optical definitions we have determined here. All Seyfert 1s, 17/21=81% of Seyfert 1.2-1.9s and 23/37=62% of Seyfert 2s have their optical classifications as AGN confirmed in X-rays. For LINERs, 2/10=20% have  $L_X > 10^{42}$  ergs $^{-1}$  as do 3/18=17% composite H II/AGN galaxies. Finally, none of the 13 H II galaxies present an X-ray luminosity greater than  $10^{42}$  ergs $^{-1}$ .

Table 5 presents the relative number of each optical class that would be solely selected by the X-ray luminosity. Here we also show how adding  $N_H$  information might aid in determining AGN activity in X-rays, given in columns 4 and 6, as heavily absorbed sources are strong candidates for being AGN. We chose an  $N_H$  cut off of  $\geq 10^{23}$  cm $^{-2}$  as none of the pure H II galaxies in our sample exhibit absorption above this level. We also explore the use of  $10^{41}$  ergs $^{-1}$  as an effective discriminator for AGN activity in columns 5 and 6.

In both limiting luminosities, adding the  $N_H$  information increases the number of AGN selected (from 56 to 64 for  $L_X > 10^{42}$  ergs $^{-1}$  and from 64 to 69 for  $L_X > 10^{41}$  ergs $^{-1}$ ), and does not add to the number of non-AGN, except for two additional LINERs which probably harbour an AGN. We should also note that two pure H II defined galaxies, NGC 1482 and NGC 1808 display a large amount of absorption in their X-ray spectra ( $N_H \simeq 9 \times 10^{22}$  cm $^{-2}$ ). Though this is slightly less than our  $10^{23}$  cm $^{-2}$  criterion above, it is still a strong indication that these galaxies may host an AGN. It is possible though, that these don't host an AGN, and that H II galaxies can be heavily obscured.

Lowering the X-ray luminosity to  $10^{41}$  ergs $^{-1}$  includes a further eight optical AGN types, with the inclusion of only two H II galaxies, which represents a 20% contamination level for the  $\log_{10}(L_X/\text{ergs}^{-1}) = 41\text{--}42$  range. This lower luminosity limit also includes a further two Compton thick sources. This shows that a lower X-ray luminosity of  $10^{41}$  ergs $^{-1}$  is an effective discriminator for AGN activity.

Fig. 5 shows the BPT diagrams of Fig. 1, but with X-ray luminosity indicated. Here it can be seen that most of the galaxies with  $L_X \geq 10^{42}$  ergs $^{-1}$  lie in the AGN regions of these diagrams. 8/60 (=13%) galaxies have  $L_X \geq 10^{42}$  ergs $^{-1}$  (observed), but are not unambiguous Seyferts (i.e. Seyfert 1-1.9s or galaxies with a Seyfert 2 classification from all three diagrams). We note VV705, ESO286-IG019, ESO148-IG002, NGC7213 on these diagrams as being X-ray luminous AGN, but with H II line ratios. VV705 and ESO286-IG019 are classed as H II/AGN composite galaxies using diagram 1, which supersedes the H II classification in the other two diagrams. ESO148-IG002 and NGC7213 are classified as H II on diagrams 1 and 2, but as Seyfert 2 and LINER respectively on diagram 3. We call ESO148-IG002 a H II/AGN composite and NGC7213 an H II/LINER. Furthermore, NGC 4388 and MCG 03-58-007 are Sy2/LINERs from their optical line ratios, NGC 6240 is a pure LINER and NGC 6552 has no line ratios available for classifications, but all of these sources are unambiguously powered by an AGN due to their X-ray luminosity. Overall, the X-ray luminosity is in agreement with the optical classification.

**Table 5.** The number of each optical type that would be selected using various X-ray information. ‘CT sources’ are X-ray sources that are Compton thick. Column (1) gives the optical type; Column (2) gives the number in our *XMM-Newton* sub-sample; Column (3) gives the number that would be selected with  $L_X > 10^{42}$  ergs $^{-1}$ ; Column (4) gives the number that would be selected with  $L_X > 10^{42}$  ergs $^{-1}$  OR  $N_H > 10^{23}$  cm $^{-2}$ ; Column (5) gives the number that would be selected with  $L_X > 10^{41}$  ergs $^{-1}$ ; Column (6) gives the number that would be selected with  $L_X > 10^{41}$  ergs $^{-1}$  OR  $N_H > 10^{23}$  cm $^{-2}$ .  $L_X$  is the observed 2-10 keV luminosity

Type	Number				
(1)	this sample (2)	$L_X$ (3)	$L_X + N_H$ (4)	$L_X$ (5)	$L_X + N_H$ (6)
Sy 1	12	12	12	12	12
Sy 1.2-1.9	21	17	18	18	19
Sy 2	37	23	29	27	31
Non Sy HBLR	8	4	5	7	7
All Sy+HBLR	<b>78</b>	<b>56</b>	<b>64</b>	<b>64</b>	<b>69</b>
LINERs	10	2	4	5	5
Sy 2/LINERs	2	1	1	2	2
H II	13	0	0	2	2
H II/AGN	18	3	3	5	5
CT sources	16	11		13	

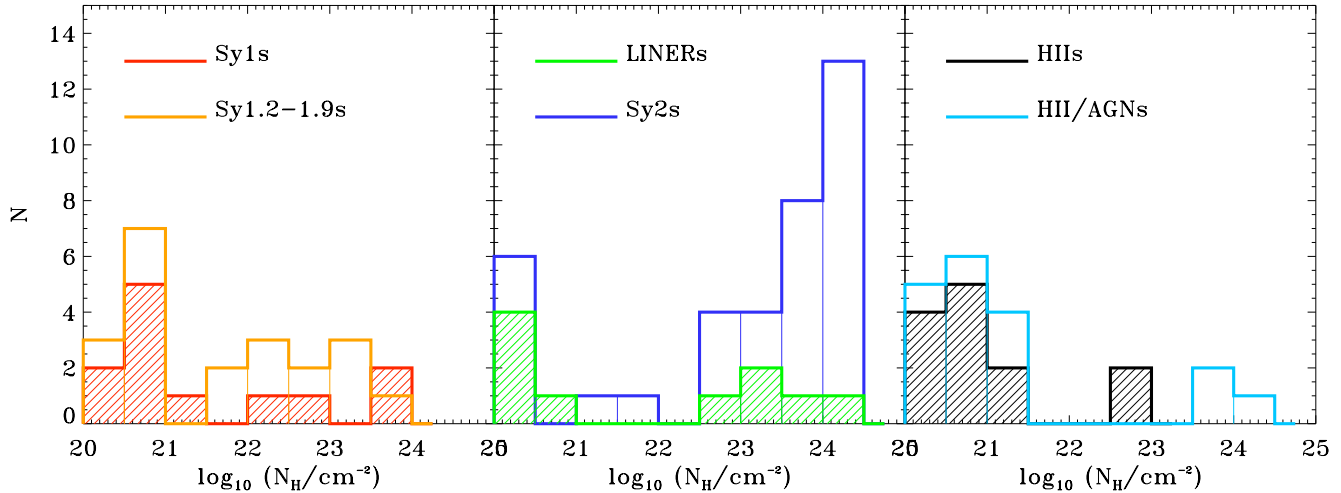
#### 4.1 Continuum

Fig. 6 gives the distribution of the X-ray power-law index,  $\Gamma$ , for the various optical types. We have grouped H II galaxies, H II/AGN composite galaxies and LINERs into one non-Seyfert category, Seyfert 1-1.9s into another category and Seyfert 2s into the last category. We use the maximum likelihood method of Maccacaro et al. (1988) to determine both the mean and the intrinsic dispersion for each of these distributions, accounting for the measurement errors. We find that for non-Seyferts,  $\langle \Gamma \rangle = 1.78^{+0.07}_{-0.08}$  and  $\sigma = 0.07^{+0.06}_{-0.07}$ , for Seyfert 1-1.9s,  $\langle \Gamma \rangle = 1.83^{+0.06}_{-0.06}$  and  $\sigma = 0.29^{+0.05}_{-0.06}$  and for Seyfert 2s,  $\langle \Gamma \rangle = 1.90^{+0.16}_{-0.17}$  and  $\sigma = 0.34^{+0.11}_{-0.16}$ . Statistically, we find that there is no difference in  $\Gamma$  between the different optical AGN types. This is in general support of AGN unification schemes as it suggests that the intrinsic properties of the central engines of Seyfert 1s and 2s are the same. On the other hand, the spectral properties of non-Seyferts are more uniform, showing no significant intrinsic dispersion in their X-ray spectral indices, in contrast to Seyferts.

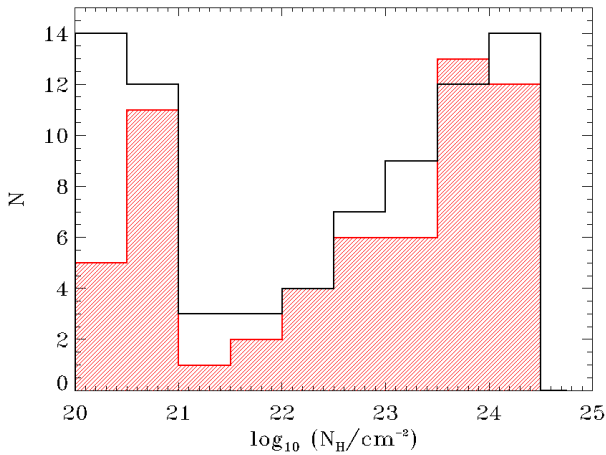
#### 4.2 Obscuration

Fig. 7 plots the distribution of neutral absorbing columns that were detected in the *XMM-Newton* spectra. As expected Seyfert 2 galaxies exhibit the largest amounts of absorption in their spectra with an average  $\log_{10} N_H = 23.08$ , whereas Seyfert 1s have an average  $\log_{10} N_H = 21.42$  and Seyfert 1.2-1.9s have an average  $\log_{10} N_H = 21.64$ . Nonetheless we do note that a naive interpretation of optical broad line AGN as being X-ray unobscured and narrow lined AGN as being X-ray obscured is incorrect, as 8/37 ( $22 \pm 7\%$ )





**Figure 7.**  $N_H$  distribution of the sources by optical type. Left panel - Seyfert 1s (red) and Seyfert 1.2-1.9 galaxies (yellow). Middle panel - Seyfert 2 galaxies (blue) and LINERs (green). Right panel - H II galaxies (black) and H II/AGN composites (light blue). Seyfert 1s and Seyfert 1.2-1.9s show very similar absorption distributions to each other, while a few of each class show heavy X-ray absorption. Seyfert 2s are mostly heavily absorbed, though a few sources show minimal X-ray absorption. The LINER population has both obscured and unobscured sources. H II and H II/AGN composites present similar distributions to each other, mostly unobscured, though with some exceptions.



**Figure 8.**  $N_H$  distribution for optically defined AGN (black) and X-ray luminous ( $L_X > 10^{42}$  erg s $^{-1}$ ) AGN (red).

sources ( $32/78 = 41\%$ ) over X-ray luminous sources ( $19/60 = 32\%$ ). In paper I we also showed that the obscured fraction for X-ray sources decreases for luminosities less than  $10^{42}$  erg s $^{-1}$ . It follows then that if one selects sources only above this luminosity there is a bias against lower absorbed sources.

We can investigate directly the variation of the obscured fraction for optically defined AGN with both intrinsic X-ray and 12  $\mu$ m luminosity. Fig. 9 presents the scatter of  $N_H$  against  $L_{12\mu m}$  and  $L_X$ , the obscured fraction, defined as the ratio of the number of AGN with  $N_H > 10^{22}$  cm $^{-2}$  to the total number of AGN for each luminosity bin and the Compton thick fraction. We choose to bin in equal steps of luminosity in logarithmic space. The errors on this plot represent

68% confidence intervals and have been calculated using a Bayesian method particularly useful for fractions at or close to 0 or 1 (described earlier in the text). The lone vertical error bars represent 68 % confidence intervals on fractions that have been calculated to be 0 or 1. We also plot the obscured fraction against X-ray luminosity as presented by Burlon et al. (2010) from their X-ray luminosity function analysis of *Swift*/BAT data for comparison. As the ratio of 15-55 keV fluxes to the 2-10 keV flux is approximately equal to 1 for a model power-law with  $\Gamma = 1.9$ , we do not scale the X-ray luminosity. The hard X-ray samples extend to higher X-ray luminosity than the 12  $\mu$ m sample, but the 12  $\mu$ m sample probes to lower X-ray luminosity. Our results agree very well here, despite different wavelength selections, and support not only a decrease in the obscured fraction at high luminosities, but also at low luminosities. The Compton thick fraction shows a similar behaviour in X-ray luminosity, though the statistics are not as good. The variation of the obscured fraction with 12  $\mu$ m luminosity also hints at a decrease at higher luminosities and possibly at lower luminosities, however, the simplest case of non-varying obscured fraction fits the data too. We do see a hint that the Compton thick fraction is dependent on 12  $\mu$ m luminosity though, suggesting that obscuration is in fact also dependent on 12  $\mu$ m luminosity.

From our analysis of the *XMM-Newton* spectra of these galaxies, we found a total of 16 Compton thick sources in our sample. All but three of these are optically defined as Seyfert 2, two are H II/AGN composites (NGC 3690 and ESO 148-IG 002), and the final source, NGC 6552, has not been optically classified here. NGC 6552 is classified as a Seyfert 2 however, by de Grijs et al. (1992), though they do not present line ratio data. The Compton thick nature of NGC 6552 was serendipitously discovered by Reynolds et al. (1994) and Fukazawa et al. (1994) with an *ASCA* observation which shows a reflection dominated spectrum and

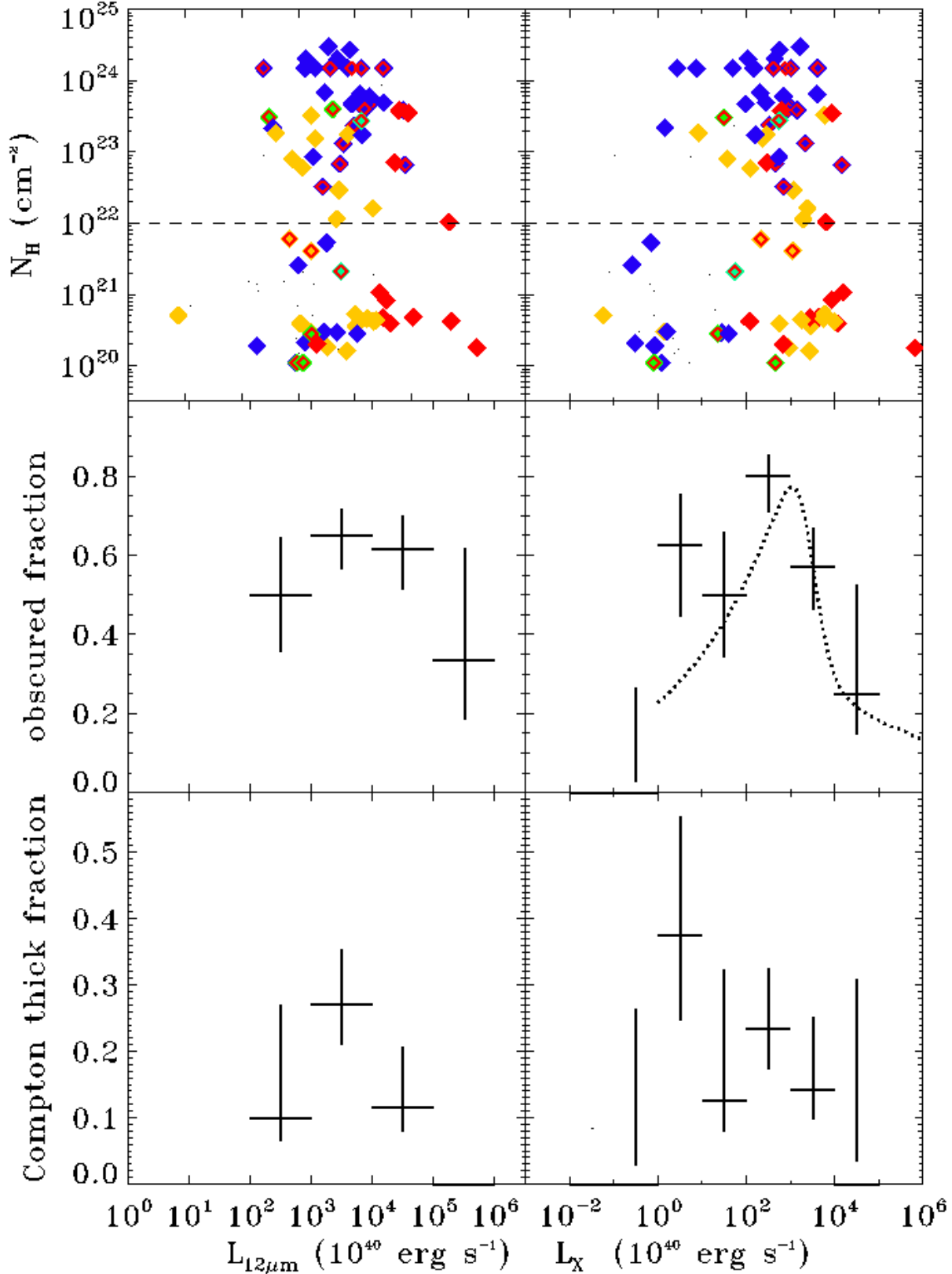


**Figure 9.**  $N_{\text{H}}$ , obscured fraction and Compton thick fraction versus  $12\mu\text{m}$  and intrinsic 2-10 keV luminosity, for AGN types only (non-AGN plotted as dots). Red, yellow and blue diamonds are Seyfert 1s, 1.2-1.9s and 2s respectively, whereas green diamonds are LINERs with an HBLR. Red outlines indicate an HBLR detected in the source. Obscured and Compton thick fractions are calculated in equal logarithmic luminosity bins, as the number of sources with  $N_{\text{H}} > 10^{22} \text{ cm}^{-2}$  divided by the total number of sources in that bin, where more than one source exists per bin. The dotted line in the middle right panel is that from Burlon, et al, from their X-ray luminosity function analysis of *Swift*/BAT data.

it also has a HBLR revealed in optical spectropolarimetry (Tran 2001). Thus, all of our Compton thick sources are AGN. Combining optical and X-ray selection, we find a total of 82 AGN in this sample, which gives us 16/82 ( $20 \pm 4\%$ ) Compton thick AGN in this sample with 51/82 ( $62 \pm 5\%$ ) obscured AGN ( $N_H \geq 10^{22} \text{ cm}^{-2}$ ).

Combining X-ray data with data at other wavelengths has been used previously to assess the Compton thick nature of AGN. Bassani et al. (1999) use the ratio of the X-ray flux to [O III] line flux, known as the ‘T’ ratio, to pick out potentially Compton thick candidates not recognised in their X-ray spectra alone. The [O III] line is thought to be an isotropic indicator of AGN strength as it is produced in the NLR. However this line is also subjected to extinction along the line of sight and a reddening correction is often applied which is derived from the Balmer decrement. Here we investigate this ratio and its effectiveness at identifying Compton thick AGN. Fig. 10 presents the distribution of this ratio for measured Compton thin (black) and thick (red) sources. We show this for the observed [O III] flux and the extinction corrected [O III] flux, for Seyfert 2s alone, and for all Seyferts. We present the means and standard deviations of these distributions in Table 6. Although it can be seen that Compton thick AGN have on average a lower T ratio than Compton thin AGN, the ratio does not separate Compton thick sources from the Compton thin population completely in any case, and many Compton thin AGN have low T ratios. We investigate the Seyferts which are not directly measured to be Compton thick, but have T ratios consistent with Compton thick obscuration ( $T < 0.1$  is generally taken to be the criterion for a candidate Compton thick AGN (Bassani et al. 1999)). Four of these sources exist, being IRASF07599+6508, MRK0273, NGC 5775 and UGC 09944. IRASF07599+6508 is a Seyfert 1 ULIRG weak in X-rays and also has a large extinction correction ( $H\alpha/H\beta=33.6$ ). MRK 0273 is a heavily obscured Seyfert 2, but not Compton thick and NGC 5775 is also a Seyfert 2 with no apparent indications of heavy obscuration in its X-ray spectrum. NGC 5775 also has an extremely large extinction correction ( $H\alpha/H\beta=126$ ). Finally UGC 09944 is also a Seyfert 2 with a low measured  $N_H$ , however, we do note an excess around 6.4 keV, which we can fit with a gaussian with high, but badly constrained EW ( $3.02^{+4.61}_{-2.51}$  keV) and unconstrained energy ( $E=6.50^{+31.4}_{-0.28}$ ). This source is potentially a Compton thick Seyfert 2. However, in 2 out of 4 cases, the extinction correction to the [O III] flux is likely to have given the source an unreliably low T. In the other two cases, one source is heavily obscured but not Compton thick, which leaves us with only one true Compton thick candidate. Our clear conclusion is that the T ratio is not a reliable Compton thick indicator, especially when uncertainties regarding extinction corrections are considered. It can however, be used to exclude the possibility of a source being Compton thick, if it has a *high* T ratio ( $> 10$  when using extinction corrected [O III]), as these sources have been shown to be almost exclusively Compton thin. We also note that our Compton thick Seyfert 2s have a range of T values that extend to higher values than Bassani et al. (1999), up to 6.3 compared to  $\sim 1$ . This may be due to our higher signal-to-noise data, with which we have managed to directly measure the Compton thickness in four of our sources, whereas Bassani et al. (1999) mostly infer the Compton thickness from a low T and high Fe K $\alpha$  EW.

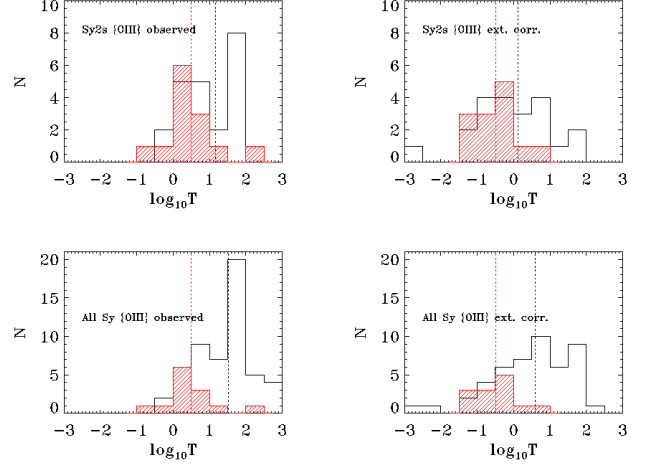


**Figure 10.** Histograms showing the distribution of the ‘T’ ratio, defined as  $F_X/F_{[\text{O III}]}$  for Compton thin (black) and Compton thick (red) sources. The top panels show only Seyfert 2, whereas the bottom panels show all Seyferts. The left panels use the observed [O III] flux, whereas the right panels use the extinction corrected [O III] flux. The X-ray flux is observed in all cases. The dotted lines show the means of the distributions, given with their standard deviations in Table 6.

**Table 6.** Mean ‘T’ ratios with their standard deviations,  $\sigma$ , for Sy 2s, all Sys, using both the observed [O III] flux and the extinction corrected [O III] flux.

Type	$\log_{10}T$ ([O III] obs.)	$\sigma$	$\log_{10}T$ ([O III] ext. corr.)	$\sigma$
Compton thin Sy 2s	1.17	0.93	0.12	1.31
Compton thick Sy 2s	0.49	0.71	-0.50	0.65
Compton thin Sys	1.51	0.89	0.59	1.22
Compton thick Sys	0.49	0.71	-0.50	0.65

## 5 X-RAY - INFRARED RELATIONSHIP IN GALAXIES

Barcons et al. (1995) and McKernan et al. (2009) both find a correlation, though a non-linear one, between X-ray and *IRAS* 12  $\mu\text{m}$  luminosities of AGN. These authors attribute some of this to a contribution to the 12  $\mu\text{m}$  luminosity by emission from the host galaxy, but Barcons et al. (1995) also points to a break down of the unification scheme as this non-linear relationship implies that the covering fraction of the torus is a function of X-ray luminosity. In the top panel of Fig. 11 we plot the 12  $\mu\text{m}$  luminosity against the intrinsic X-ray luminosity for all 126 galaxies in our sample, colour coded by optical type. The dotted lines on this diagram represent  $L_{12\mu\text{m}} = L_X$ ,  $L_{12\mu\text{m}} = 100 \times L_X$  and  $L_{12\mu\text{m}} = 10^4 \times L_X$ . The X-ray luminosities have been corrected for absorption. It is clear here that the relationship between 12  $\mu\text{m}$  luminosity and X-ray luminosity is non-linear, and there is a large scatter, even for AGN only. Star-forming galaxies also have a much larger  $L_{12\mu\text{m}}/L_X$  than AGN. The dot-dashed lines on this plot mark the  $10^{41}$  and  $10^{42} \text{ erg s}^{-1}$

X-ray luminosities, again showing that all but two galaxies with  $L_X > 10^{41}$  erg s $^{-1}$  are AGN.

The lower plot in Fig. 11 highlights the luminosities of the different type 1 Seyferts. Most striking, is the separation between Seyfert 1 galaxies and Seyfert 1.2-1.9 galaxies in 12  $\mu$ m luminosity which we discovered previously. Seyfert 1s almost exclusively have  $L_{12\mu m} > 3 \times 10^{44}$  ergs s $^{-1}$ , whereas Seyfert 1.2-1.9 have luminosities exclusively less than this.

Horst et al. (2008) find that Seyfert 1s and Seyfert 2s have the same intrinsic distribution of  $L_{MIR}/L_X$ , which is not expected from smooth dusty torus models, as the 12  $\mu$ m flux should be suppressed in edge on, Seyfert 2 type systems (Pier & Krolik 1992). This is a key result when considering 12 $\mu$ m selection, and using the 12MGS to infer properties of obscuration in local AGN, so we also test if there is any dependence between the X-ray to 12  $\mu$ m flux ratio and absorption measured in the X-ray band. In Fig. 12, we show the observed 2-10 keV flux to the 12  $\mu$ m flux against the neutral column density measured. The dashed line we plot is the ratio of the 12  $\mu$ m to 2-10 keV bolometric corrections for AGN,  $\kappa_{12\mu m}/\kappa_{2-10keV}$ . We use the average  $\kappa_{2-10keV}$ , from Vasudevan & Fabian (2007) with the total 1 dex spread that they present, and we calculate  $\kappa_{12\mu m}$ , from the bolometric luminosities of the AGN given in Spinoglio et al. (1995) which we calculate to be 10.1, with a standard deviation of 0.34 dex. This gives  $\kappa_{12\mu m}/\kappa_{2-10keV} = 0.40$  with a spread of 0.6 dex represented by the dotted line in each plot. This is consistent with the results of Horst et al. (2008) and their nuclear 12.3  $\mu$ m observations (0.42 for Seyfert 1s and 0.36 for Seyfert 2s). The bolometric ratio is also plotted as a function of the X-ray column density, where the 2-10 keV contribution has been suppressed by a factor calculated from our Monte-Carlo model presented in paper I. We place AGN found to be Compton thick in our previous analysis at  $N_H = 1.5 \times 10^{24}$  cm $^{-2}$ , which is a lower limit to their  $N_H$ . The symbols are colour coded to represent their optical types.

We find that most Seyfert 1s have X-ray to MIR flux ratios consistent with the bolometric corrections, as do some Seyfert 2s, however, most Seyfert 2s have a lower than expected ratio, even when taking the suppression of the X-ray flux by absorbing columns into account. Star-forming galaxies are seen to have a much lower ratio than AGN. It is likely that the lower than expected X-ray to MIR flux ratio seen in Seyfert 2s is due to MIR dust emission from their host galaxies which have been heated by star formation.

## 6 DISCUSSION

### 6.1 X-ray properties of Seyfert galaxies

We have presented the average intrinsic X-ray ( $L_X$  and  $\Gamma$ ) and X-ray absorption ( $N_H$ ) properties of our sample for each optical class that we have determined here, be it Seyfert 1s, Seyfert 1.2-1.9s, Seyfert 2s, LINERs, H II galaxies or composite H II/AGN galaxies. For Seyfert galaxies, much of our existing knowledge of these properties comes from analysis of the X-ray selected sample of Piccinotti et al. (1982). Here we can compare the properties we derive from our MIR selected sample to those earlier results. The Seyfert 1s in our sample have an average intrinsic X-ray luminosity of  $\log_{10} L_X = 43.3 \pm 0.72$ ,  $\langle \Gamma \rangle = 1.83^{+0.06}_{-0.06}$  and  $\sigma_\Gamma = 0.29^{+0.05}_{-0.06}$

( $\langle \Gamma \rangle$  for Sy 1-1.9s) and  $\log_{10} N_H = 21.42$ . For the X-ray selected sample of Seyfert 1s measured by ASCA from Nandra et al. (1997), they find an average  $\log_{10} L_X = 43.3 \pm 0.91$  and  $\langle \Gamma \rangle = 1.90 \pm 0.17$  and  $\sigma_\Gamma = 0.15 \pm 0.05$ . Our mean luminosities are the same, and our  $\langle \Gamma \rangle$  are consistent with each other, however, we find a significantly broader distribution of  $\Gamma$  than in the Nandra et al. (1997) sample. The Seyfert 2s in our sample have an average intrinsic X-ray luminosity of  $\log_{10} L_X = 42.0 \pm 1.29$ ,  $\langle \Gamma \rangle = 1.90^{+0.16}_{-0.17}$  and  $\sigma_\Gamma = 0.34^{+0.11}_{-0.16}$  and  $\log_{10} N_H = 23.08$ . ASCA results from Turner et al. (1997) for Seyfert 2s, derived from the same X-ray selected sample as Nandra et al. (1997) give  $\langle \Gamma \rangle = 2.09 \pm 0.02$ . However, due to the complexities present in fitting the X-ray spectra, of Seyfert 2 galaxies, such as complex absorption, it is not straightforward to compare our results with theirs.

For LINERs, the most comprehensive X-ray spectral study so far has been done by González-Martín et al. (2009) based on a multi-wavelength selection. The LINERs in our sample have an average intrinsic X-ray luminosity of  $\log_{10} L_X = 40.8 \pm 1.63$  and an average  $\log_{10} N_H = 21.92$ . González-Martín et al. (2009) find that the average 2-10 keV luminosity of their XMM-Newton sample is  $\log_{10} L_X = 40.3 \pm 1.5$  and  $\log_{10} N_H = 21.93$ . These parameters are very similar between the two works, despite differing selection techniques, which may suggest homogeneity among the LINER class.

For the H II (H II/AGN composite) galaxies, we find the average  $\log_{10} L_X = 40.0 \pm 0.93$  ( $40.5 \pm 1.42$ ) and  $\log_{10} N_H = 21.0$  (21.2). For the analysis of  $\Gamma$  we group together LINERs, H II galaxies, and H II/AGN composites and find that  $\langle \Gamma \rangle = 1.78^{+0.07}_{-0.08}$  and  $\sigma_\Gamma = 0.07^{+0.06}_{-0.07}$  for these galaxies. Ptak et al. (1999) presented an X-ray spectral analysis of a sample of low-luminosity AGN, which consisted mostly of LINERs and starbursts, observed with ASCA. From their power-law spectral fits they find  $\langle \Gamma \rangle = 1.71 \pm 0.41$ , which is consistent with our results from a similar mix of galaxies.

### 6.2 AGN selection and classification

We have found that our X-ray data generally support MIR AGN selection, as we have found a higher fraction of obscured AGN ( $62 \pm 5\%$ ) than optically selected samples ( $\sim 50\%$ , eg, Cappi et al. 2006) and hard X-ray selected ( $50\%$ , Tueller et al. 2008) AGN samples, as well as a higher Compton fraction (discussed below).

As for finding AGN in non-Seyfert galaxies, we find an X-ray luminosity in excess of  $10^{42}$  ergs $^{-1}$  in 17% of the composite H II/AGN defined galaxies, whereas we find no such indications in any of the pure H II defined galaxies. The H II/AGN composites also have on average a greater [O III] luminosity than H II galaxies. As the [O III] line is used in the classification of these galaxies, this may be interpreted straightforwardly as a selection effect. However, it is mostly the [N II] line which is used to distinguish these from pure H II defined galaxies, so a greater [O III] luminosity indicates AGN activity in the H II/AGN composite galaxies. From infrared SED fitting, Patel et al. (2010) find 3% of composite galaxies in the SWIRE, XMM-LSS and Lockman Hole surveys require an AGN component, suggesting that X-ray observations are more efficient at identifying AGN activity.

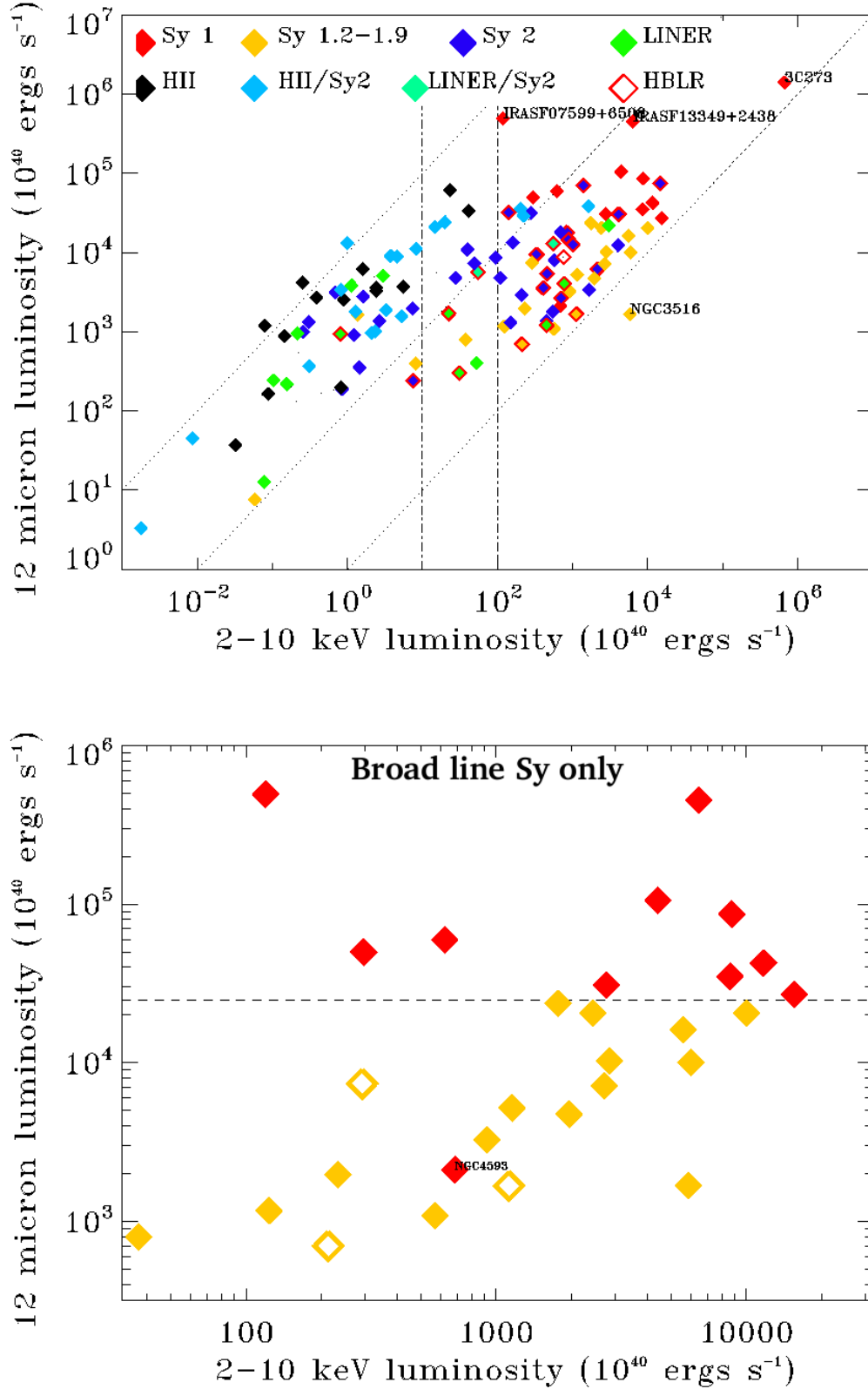


**Figure 11.** 12 $\mu\text{m}$  luminosity versus intrinsic 2-10 keV luminosity for our sample. (top) The dotted lines on this diagram represent  $L_{12\mu\text{m}} = L_X$ ,  $L_{12\mu\text{m}} = 100 \times L_X$  and  $L_{12\mu\text{m}} = 10^4 \times L_X$ . (bottom) Only Seyfert 1-1.9 (broad line Sy) types are plotted here. We show Sy 1.8-1.9s as open yellow symbols.

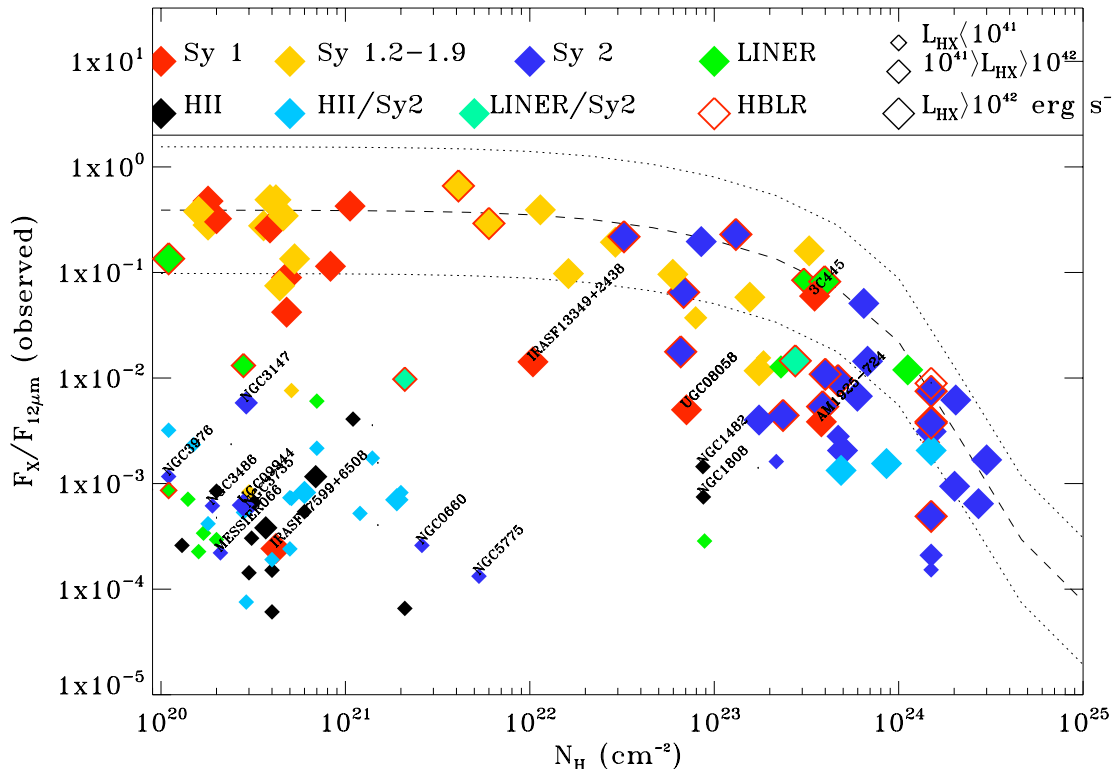


**Figure 12.** Observed 2-10 keV to 12 $\mu$ m flux ratio versus measured column density for our sample. The colour of each symbol represents the optical type of galaxy, whereas the size of the symbol represents the X-ray luminosity of the galaxy. The dashed line is the ratio of the respective bolometric corrections for AGN for the quantities given, which we find to be  $0.40 \pm 0.6$  dex, where the dotted lines indicate the spread in this value. The ratio is also plotted as a function of the X-ray column density, where the 2-10 keV contribution has been suppressed by a factor calculated from our Monte-Carlo model. Named are galaxies where interesting cases where the X-ray obscuration is in contradiction to the optical type (eg. obscured Seyfert 1s)

Our findings support such a ‘composite’ classification based on optical line ratios.

We also find evidence for AGN activity in a large number (40%) of LINERs from the X-ray data. This includes NGC 6240, well known for its LINER classification in the optical, but unambiguously powered by a heavily obscured AGN in the X-rays, as *Beppo-SAX* showed with the detection of a hard component (Mitsuda 1995). However González-Martín et al. (2009) have recently reported that a much larger fraction, 80%, show indications for AGN activity in LINERs. However, as well as X-ray luminosity and absorption, they also use X-ray morphology, and data at other wavelengths to suggest AGN activity. By contrast, Goulding & Alexander (2009) find only a 25% AGN fraction in IR bright LINERs from the detection of the [NeV] line. It would seem that LINERs are mostly low luminosity AGN, but that in a few cases, they are more powerful Compton thick AGN. The decline in the LINER fraction of Seyfert and LINER galaxies with  $12\text{ }\mu\text{m}$  and X-ray luminosity also supports this conclusion.

### 6.3 AGN obscuration

The most commonly compared study of the distribution of X-ray absorbing columns in AGN is that by Risaliti, Maiolino & Salvati (1999), who showed that  $\sim 75\%$  of

their optically selected Seyfert 2s were heavily absorbed ( $N_{\text{H}} > 10^{23} \text{ cm}^{-2}$ ) and  $\sim 50\%$  were Compton thick. The authors applied an [O III] flux cut off of  $4 \times 10^{-13} \text{ erg s}^{-1} \text{ cm}^{-2}$  to their sample however, leaving them with a sample of bright Seyfert 2s, so a direct comparison to their work is not straightforward. However, for the [O III] fluxes we have compiled, if we apply the same cut off and include Seyfert 1.8 and 1.9s, we find that  $75 \pm 8\%$  of them are heavily absorbed and  $39 \pm 9\%$  are Compton thick. This agrees well with the Risaliti et al. (1999) study, though with a smaller, but not significantly so, proportion of heavily obscured Seyfert 2s being Compton thick. Furthermore, some of the Seyfert 2s in the Risaliti et al. (1999) study have since been shown to be probably not Compton thick (Treister et al. 2009), so the true Compton thick fraction for these bright Seyferts is probably closer to  $\sim 40\%$  as our results suggest.

We find a Compton thick fraction of  $20 \pm 4\%$  in the 12  $\mu\text{m}$  sample. Akylas & Georgantopoulos (2009) find 3/38 (8%) of their optically selected sample of Seyferts, which has a similar range in  $L_X$  to our sample ( $10^{38}$  to  $10^{43}$   $\text{ergs}^{-1}$ ), to be Compton thick from direct measurements of the  $N_{\text{H}}$ . However they also note a low T ratio in many other AGN in their sample, which, if they include these as inferred Compton thick objects, would increase their Compton thick fraction to 20%, in rough agreement with our statistic. Their 8% statistic is still within  $3\text{-}\sigma$  of our own though and can thus

be considered as consistent with our results. Cappi et al. (2006) also find a 20% Compton thick fraction from their analysis of the same survey. The hard X-ray selected samples also reveal a significantly lower ( $>3\sigma$ ) Compton thick fraction ( $\sim 4\%$ , eg, Beckmann et al. 2009). In paper I we showed the effect of heavy obscuration on X-ray transmission above 10 keV. At a column density of  $\sim 4 \times 10^{24} \text{ cm}^{-2}$  the observed flux is half that of the intrinsic flux in the 10-40 keV band, and at  $\sim 10^{25} \text{ cm}^{-2}$  it is 10% of that level, presenting a real bias against heavily obscured systems in hard X-ray surveys, and indeed Malizia et al. (2009) show that when considering only the closest *INTEGRAL* sources, the Compton thick fraction they derive is in better agreement. For the *Swift*/*BAT* survey, Burlon et al. (2010) account for the selection bias in the hard X-ray band, and recover a 20% Compton thick AGN fraction in doing so.

We have shown however, that using the T ratio to consider an AGN as Compton thick is misleading in many cases, especially when taking the extinction correction into account. We found that 2/4 Seyferts with a T ratio consistent with Compton thick obscuration have extremely large Balmer decrements leading to huge extinction corrections, and probably unreliable T ratios. LaMassa et al. (2010) investigated the reddening correction of [O III] for the 12MGS finding that applying the correction based on the Balmer decrement widened the dispersion in the flux ratio of the [O III] line to other isotropic indicators, whereas the dispersion tightened for their optically selected sample. They conclude that the extinction correction, which is based on heterogeneous literature values for the 12MGS, overestimate the reddening due to dust. One Seyfert however, UGC09944, does seem to be a reliable Compton thick candidate based on the T ratio, shown from a large EW but not well constrained Fe K $\alpha$  line. We do find though that a source with a high T ratio can be excluded from being Compton thick as almost all sources which present a high T ratio are Compton thin.

#### 6.4 AGN unification

Our analysis of the  $\Gamma$  distribution of Seyfert 1-1.9 and Seyfert 2s shows that there is not a significant difference in the spectral slopes of the two classes, suggesting that the power generation mechanism in the two classes is essentially the same, and thus in support of the unification of the Seyfert types. Several authors have reported a difference in the two distributions, finding that Seyfert 2s tend to have a harder spectral slope (eg, Tueller et al. 2008; Middleton et al. 2008). These studies have the advantage of data above 10 keV and therefore are less subjected to absorption effects. However, Malizia et al. (2003) also make use of data above 10 keV, and although they find a systematic difference between the two types initially, this difference disappears when more complex absorption models are used to model the Seyfert 2 data. Dadina (2008) also draws the same conclusion from *Beppo-SAX* data.

Arguing against unification schemes are the finding of cases where Seyfert 1s are X-ray absorbed and Seyfert 2s are X-ray unabsorbed, and finding that Seyfert 1s are intrinsically more powerful than Seyfert 2s at 12  $\mu\text{m}$ , [O III] and X-ray wavelengths. Furthermore, we also show that AGN obscuration depends on X-ray luminosity, finding that

rather than declining with  $L_X$ , the obscured fraction peaks at  $L_X \sim 10^{42} \text{ erg s}^{-1}$ . Other authors have previously reported that the obscured fraction of AGN decreases at high luminosities (eg. Ueda et al. 2003; Hasinger 2008), but their samples do not generally extend into the lower luminosity range probed by the 12MGS. The decline in the obscured fraction at high luminosities is supported by the decline we see in the Seyfert 2 fraction above  $\sim 10^{43} \text{ erg s}^{-1}$ . This has also been previously reported (e.g. Simpson 2005, in [O III] luminosity), though this is still a subject of debate (see Lawrence & Elvis 2010, for a discussion on this). As for the decline in the obscured fraction towards low luminosities, Akylas & Georgantopoulos (2009) also find evidence for less obscuration at low luminosities, as do Zhang et al. (2009), both for nearby AGN. Burlon et al. (2010) similarly find a peak in the obscured fraction for the *Swift*/*BAT* selected AGN from luminosity function analysis. The variation of the obscured fraction with 12  $\mu\text{m}$  luminosity is not as statistically significant as seen in X-rays, and is consistent with a non-varying obscured fraction, but better statistics are needed to test this definitively. The Compton thick fraction does, however, seem to vary with 12  $\mu\text{m}$  luminosity, suggesting that obscuration does in fact depend on 12  $\mu\text{m}$  luminosity as well as X-ray luminosity.

Hopkins et al. (2009) attribute the disappearance of the BLR to low accretion rate, radiatively inefficient systems as observationally found by Nicastro et al. (2003) who show that the detection rate of HBLRs in Seyfert 2s decreases with accretion rate. Modelling of outflows in low luminosity AGN by Elitzur & Shlosman (2006) predicts that both the torus and the BLRs disappear at low bolometric luminosities, which would explain both the decline we see in the obscured fraction at low X-ray luminosities and the lower incidence of HBLRs at low X-ray luminosities.

Another interesting difference our data reveal is that strict Seyfert 1s have a distinctly different 12  $\mu\text{m}$  luminosity distribution from the intermediate type 1.2-1.9s Seyferts, which is shown to be highly statistically significant from a K-S test. This is also seen in the decline of the intermediate type fraction with 12  $\mu\text{m}$  luminosity. The progression from strict type 1 through to type 1.5 is dependent on the ratio of the total H $\beta$  flux to the [O III] flux, i.e. the relative strengths of the BLR and NLR, where Seyfert 1.5s have the weakest BLR to NLR ratio. The difference in the relative strengths between these Seyfert sub-types may be due to reddening of the BLR, or due to an intrinsic difference in the ionising flux (Tran et al. 1992). A difference in 12  $\mu\text{m}$  luminosity between the Seyfert 1s and intermediate Seyferts suggests that the 12  $\mu\text{m}$  luminosity is in some way connected to the relative strength of the BLR to the NLR in unobscured AGN. It should be noted that the X-ray luminosity distributions of Seyfert 1s and intermediate Seyferts are not shown to be significantly different. If we then presume that the X-ray luminosity is an indicator of nuclear power; higher 12  $\mu\text{m}$  luminosities in Seyfert 1s might suggest a higher covering fraction of the torus in Seyfert 1s with respect to intermediate Seyferts. This in turn suggests that the strength of the BLR is dependent on the torus covering fraction, and implies an origin in the torus for the BLR. This supports the model presented by Gaskell (2009), which describes the BLR as the inner part of the torus, where material has lost angular momentum and the dust has sublimated. This sub-

sequently forms into an accretion disk and is accreted by the black hole.

In conclusion, it seems that our data suggest some intrinsic link between the torus, the BLRs and the accretion disk, and finds good cause for modifications to be made to the simplest AGN unification schemes.

### 6.5 Implications for the X-ray background

The predictions of the recent X-ray background synthesis models of Gilli et al. (2007) claim to match the observed Compton thick fraction as found by hard X-ray telescopes. However, since publication of the hard X-ray samples, the Compton thick fraction has fallen due to ongoing observations (Beckmann et al. 2009). Treister et al. (2009) argue that the discrepancy between observations and models is due to degeneracies in the models used to fit the background spectrum, in particular, the normalisation of the Compton reflection component. They argue that only direct observations can be used to constrain the properties of Compton thick AGN in the local universe. Alternatively, or in addition, consideration of blazars in the synthesis models lead to a lower required CT AGN fraction (Draper & Ballantyne 2009). As we have shown, the 12MGS is well suited to directly constraining the Compton thick fraction of AGN in the local universe due to its representative nature and the relative lack of bias towards heavily obscured systems, so we conclude that the true Compton thick fraction of local AGN is only  $\sim 20\%$ .

Furthermore, the intrinsic dispersion on  $\Gamma$  is an important parameter when considering XRB models. Gilli et al. (2007) directly investigated the effect of introducing a non zero  $\sigma_\Gamma$  into the synthesis models, and evaluated the effect of varying the size of the dispersion. They found that the larger the dispersion, the greater contribution to the 30 keV peak from unobscured AGN there was. For their baseline model they use  $\sigma_\Gamma = 0.2$  based on results from Mateos et al. (2005) on faint sources in the Lockman Hole. Here we find that for local AGN,  $\sigma_\Gamma \simeq 0.3$ , which would introduce a greater contribution to the 30 keV peak from unobscured AGN than the Gilli et al models produce, and hence require a smaller contribution from Compton thick AGN.

### 6.6 Implications for high redshift studies

Mid-IR observations by *Spitzer* are being used extensively for deep field, high redshift studies of AGN. This is due to the fact that much of the reprocessed primary energy of the AGN is re-emitted in the mid-IR. Our local study at 12  $\mu\text{m}$  corresponds exactly to the *Spitzer/MIPS* 24  $\mu\text{m}$  selected sources at  $z=1$ , and provides valuable insight into the nature of these sources. Building on results from Horst et al. (2008) and finding that 12  $\mu\text{m}$  selected AGN contain a higher fraction of Compton thick sources than optically or hard X-ray selected samples, we have concluded that mid-IR selection is indeed ideally suited to selecting AGN and is relatively unbiased against obscuration, bolstering these deep field efforts. We have found that using a lower X-ray luminosity of  $10^{41} \text{ erg s}^{-1}$  rather than  $10^{42} \text{ erg s}^{-1}$  will increase the number of AGN selected in X-ray surveys, with minimal inclusion of star forming galaxies, which is valuable information for the high- $z$  searches.

Additionally, the 24  $\mu\text{m}$  band of *Spitzer/MIPS* is often used to select ‘infrared excess’ (IRX) sources, where the flux in the 24  $\mu\text{m}$  band is in excess compared to a wavelength which is more subjected to absorption, such as the optical R band or X-rays (eg. Fiore et al. 2008; Georgantopoulos et al. 2009). These IRX sources are candidates for high- $z$  Compton thick AGN, but as we have shown for our local sources, there are cases where low X-ray to mid-IR AGN (infrared excess sources) are not in fact heavily obscured and have intrinsically low ratios (eg. IRASF 07599+6508, NGC 3147, IRASF 01475-0740.). Recently Georgakakis et al. (2010) investigated the nature of  $z \sim 2$  IRX sources and showed that only a small fraction of them displayed tentative evidence for being Compton thick.

## 7 CONCLUSIONS

In summary, we have uniformly determined the optical types for the 126 galaxies that form a sub-sample of the 12MGS, for which we have good X-ray data from paper I using BPT line ratio diagnostics. We have conducted a study comparing the optical and X-ray selection methods and have also characterised the optical types in the X-ray and we have investigated X-ray properties of the sample by optical type.

The main conclusions from this study have been that:

- strict Seyfert 1s are distinctly more powerful at X-ray luminosities than Seyfert 2s and distinctly more powerful at 12  $\mu\text{m}$  luminosities than both intermediate Seyferts and Seyfert 2s.
- Seyfert 2 galaxies with a detection of an HBLR show a significantly higher X-ray luminosity than those without a detection, supporting the findings of Tran (2003).
- The Seyfert 2 fraction of Seyfert galaxies is a strong decreasing function of X-ray luminosity dropping from  $\sim 60\%$  to  $\sim 30\%$  at  $10^{43} \text{ erg s}^{-1}$ .
- our X-ray data are in general support of the classification of AGN using optical emission lines, though we find seven ‘hidden’ AGN from X-ray data in galaxies optically defined as H II/AGN composite or LINER, and two further candidates in the H II defined NGC 1482 and NGC 1808 due to their large detected absorption columns.
- H II/AGN composites show a higher average [O III] luminosity than pure H II galaxies indicating AGN power in the composites, plus 17% show X-ray indications of AGN power, supporting claims that these galaxies harbour at least a low level active nucleus.
- X-ray indications of AGN power, being heavy absorption and/or high X-ray luminosity, are found in 40% of MIR selected LINERs.
- using a lower X-ray luminosity of  $10^{41} \text{ erg s}^{-1}$ , rather than the widely used  $10^{42} \text{ erg s}^{-1}$ , to select optical AGN is effective, with only a 3% contamination rate by star-forming galaxies. Including heavily obscured X-ray sources with  $N_H > 10^{23} \text{ cm}^{-2}$  also adds to the number of AGN selected with the exclusion of star-forming galaxies.
- we find general support for AGN unification schemes due to the distribution of power-law indices,  $\Gamma$ , for Seyfert 1s and 2s being consistent with each other implying that the power generation mechanism is the same in both. We also find that on average the  $N_H$  measured in Seyfert 2s is higher than Seyfert 1s, as expected from unification schemes.

- however, in 24% of cases the absorption measured in the X-ray spectra does not correspond directly with that implied in the optical band from the visibility of the BLRs.

- a luminosity dependent modification to the AGN unified scheme is required. This is to account for the decrease in the obscured fraction at high X-ray luminosities ( $L_X > 10^{43}$  erg s<sup>-1</sup>), possibly due to the recession of the torus at these high source powers; and also a decrease in both the obscured fraction and HBLR detection at low X-ray luminosities ( $L_X < 10^{42}$  erg s<sup>-1</sup>).

- 12 micron selected galaxies contain a higher fraction of obscured ( $62 \pm 5\%$ ) and Compton thick ( $20 \pm 4\%$ ) AGN than hard X-ray and optically selected samples, supporting MIR selection as a relatively unbiased method of selecting AGN.

- use of the ‘T’ ratio to find candidate Compton thick sources can often be unreliable, partly due to large extinction corrections. We can support the use of the ratio to exclude Compton thickness though, as a high ratio almost exclusively belongs to Compton thin sources.

- our work on the locally selected 12MGS is important for high redshift AGN studies, especially for IR selected samples, as we have shown that this selection method is relatively unbiased, and that X-ray luminosity and accurate  $N_H$  information can be valuable for selecting AGN.

## 8 ACKNOWLEDGEMENTS

## REFERENCES

- Akylas A., Georgantopoulos I., 2009, *A&A*, 500, 999
- Antonucci R., 1993, *ARA&A*, 31, 473
- Armus L., Heckman T. M., Miley G. K., 1989, *ApJ*, 347, 727
- Baan W. A., Salzer J. J., Lewinter R. D., 1998, *ApJ*, 509, 633
- Baldwin J. A., Phillips M. M., Terlevich R., 1981, *PASP*, 93, 5
- Barcons X., Franceschini A., de Zotti G., Danese L., Miyaji T., 1995, *ApJ*, 455, 480
- Bassani L., Dadina M., Maiolino R., Salvati M., Risaliti G., della Ceca R., Matt G., Zamorani G., 1999, *ApJS*, 121, 473
- Beckmann V., Soldi S., Ricci C., Alfonso-Garzón J., Courvoisier T., Domingo A., Gehrels N., Lubiński P., Mas-Hesse J. M., Zdziarski A. A., 2009, *A&A*, 505, 417
- Bianchi S., Corral A., Panessa F., Barcons X., Matt G., Bassani L., Carrera F. J., Jiménez-Bailón E., 2008, *MNRAS*, pp 108–
- Brightman M., Nandra K., 2008, *MNRAS*, 390, 1241
- Brightman M., Nandra K., 2010, *ArXiv e-prints*
- Burlon D., Ajello M., Greiner J., Comastri A., Merloni A., Gehrels N., . 2010, *ArXiv e-prints*
- Cameron E., 2010, *ArXiv e-prints*
- Cappi M., Panessa F., Bassani L., Dadina M., Dicocco G., Comastri A., della Ceca R., Filippenko A. V., Gianotti F., Ho L. C., Malaguti G., Mulchaey J. S., Palumbo G. G. C., 2006, *A&AP*, 446, 459
- Corbett E. A., Kewley L., Appleton P. N., Charmandaris V., Dopita M. A., Heisler C. A., Norris R. P., Zezas A., Marston A., 2003, *ApJ*, 583, 670
- Cusumano G., La Parola V., Segreto A., Ferrigno C., Maselli A., Sbarufatti B., Romano P., Chincarini G., Giommi P., Masetti N., Moretti A., Parisi P., Tagliaferri G., 2010, *A&A*, 524, A64+
- Dadina M., 2008, *A&A*, 485, 417
- de Grijp M. H. K., Keel W. C., Miley G. K., Goudfrooij P., Lub J., 1992, *A&AS*, 96, 389
- Dopita M. A., Heisler C., Lumsden S., Bailey J., 1998, *ApJ*, 498, 570
- Draper A. R., Ballantyne D. R., 2009, *ApJ*, 707, 778
- Elitzur M., Shlosman I., 2006, *ApJL*, 648, L101
- Ferrarese L., Merritt D., 2000, *ApJL*, 539, L9
- Fiore F., Grazian A., Santini P., Puccetti S., Brusa M., Feruglio C., Fontana A., Giallongo E., Comastri A., Gruppi C., Pozzi F., Zamorani G., Vignali C., 2008, *ApJ*, 672, 94
- Fukazawa Y., Makishima K., Ebisawa K., Fabian A. C., Gendreau K. C., Ikebe Y., Iwasawa K., Kii T., Mushotzky R. F., Ohashi T., Otani C., Ricker G. R., Tamura T., Tanaka Y., Ueda Y., White N. E., 1994, *PASJ*, 46, L141
- Gaskell C. M., 2009, *New Astronomy Review*, 53, 140
- Gebhardt K., Bender R., Bower G., Dressler A., Faber S. M., Filippenko A. V., Green R., Grillmair C., Ho L. C., Kormendy J., Lauer T. R., Magorrian J., Pinkney J., Richstone D., Tremaine S., 2000, *ApJL*, 539, L13
- Georgakakis A., Rowan-Robinson M., Nandra K., Digby-North J., Perez-Gonzalez P. G., Barro G., 2010, *ArXiv e-prints*
- Georgantopoulos I., Akylas A., Georgakakis A., Rowan-Robinson M., 2009, *A&A*, 507, 747
- Ghosh H., Pogge R. W., Mathur S., Martini P., Shields J. C., 2007, *ApJ*, 656, 105
- Gilli R., Comastri A., Hasinger G., 2007, *A&A*, 463, 79
- Gonçalves A. C., Véron-Cetty M.-P., Véron P., 1999, *A&AS*, 135, 437
- González-Martín O., Masegosa J., Márquez I., Guainazzi M., Jiménez-Bailón E., 2009, *A&A*, 506, 1107
- Goulding A. D., Alexander D. M., 2009, *MNRAS*, 398, 1165
- Grier C. J., Mathur S., Ghosh H., Ferrarese L., 2010, *ArXiv e-prints*
- Hasinger G., 2008, *A&A*, 490, 905
- Heckman T. M., 1980, *A&A*, 87, 152
- Ho L. C., Filippenko A. V., Sargent W. L. W., 1997, *ApJS*, 112, 315
- Hönig S. F., Kishimoto M., Gandhi P., Smette A., Asmus D., Duschl W., Polletta M., Weigelt G., 2010, *A&A*, 515, A23+
- Hopkins P. F., Hickox R., Quataert E., Hernquist L., 2009, *MNRAS*, 398, 333
- Horst H., Gandhi P., Smette A., Duschl W. J., 2008, *A&A*, 479, 389
- Huchra J., Burg R., 1992, *ApJ*, 393, 90
- Hunt L. K., Malkan M. A., 1999, *ApJ*, 516, 660
- Kauffmann G., Heckman T. M., Tremonti C., Brinchmann J., Charlot S., White S. D. M., Ridgway S. E., Brinkmann J., Fukugita M., Hall P. B., Ivezić Ž., Richards G. T., Schneider D. P., 2003, *MNRAS*, 346, 1055
- Kewley L. J., Groves B., Kauffmann G., Heckman T., 2006, *MNRAS*, 372, 961
- Kewley L. J., Heisler C. A., Dopita M. A., Lumsden S., 2001, *ApJS*, 132, 37
- Kim D.-C., Sanders D. B., Veilleux S., Mazzarella J. M.,

- Soifer B. T., 1995, *ApJS*, 98, 129
- Kong X., Cheng F. Z., Weiss A., Charlot S., 2002, *A&A*, 396, 503
- Kopylov I. M., Lipovetskii V. A., Pronik V. I., Chuvaev K. K., 1974, *Astrophysics*, 10, 305
- Kormendy J., 1988, *ApJ*, 325, 128
- LaMassa S. M., Heckman T. M., Ptak A., Martins L., Wild V., Sonnentrucker P., 2010, *ApJ*, 720, 786
- Laor A., 2003, *ApJ*, 590, 86
- Lawrence A., Elvis M., 2010, *ArXiv e-prints*
- Maccacaro T., Gioia I. M., Wolter A., Zamorani G., Stocke J. T., 1988, *ApJ*, 326, 680
- Magorrian J., Tremaine S., Richstone D., Bender R., Bower G., Dressler A., Faber S. M., Gebhardt K., Green R., Grillmair C., Kormendy J., Lauer T., 1998, *AJ*, 115, 2285
- Maia M. A. G., da Costa L. N., Willmer C., Pellegrini P. S., Rite C., 1987, *AJ*, 93, 546
- Malizia A., Bassani L., Stephen J. B., Di Cocco G., Fiore F., Dean A. J., 2003, *ApJL*, 589, L17
- Malizia A., Stephen J. B., Bassani L., Bird A. J., Panessa F., Ubertini P., 2009, *MNRAS*, 399, 944
- Mateos S., Barcons X., Carrera F. J., Ceballos M. T., Hasinger G., Lehmann I., Fabian A. C., Streblyanska A., 2005, *A&A*, 444, 79
- McKernan B., Ford K. E. S., Chang N., Reynolds C. S., 2009, *MNRAS*, 394, 491
- Middleton M., Done C., Schurch N., 2008, *MNRAS*, 383, 1501
- Mitsuda K., 1995, in Böhringer H., Morfill G. E., Trümper J. E., eds, *Seventeenth Texas Symposium on Relativistic Astrophysics and Cosmology Vol. 759 of New York Academy Sciences Annals, ASCA Results on Active Galactic Nuclei..* pp 213–+
- Mullaney J. R., Alexander D. M., Goulding A. D., Hickox R. C., 2011, *ArXiv e-prints*
- Nandra K., George I. M., Mushotzky R. F., Turner T. J., Yaqoob T., 1997, *ApJ*, 477, 602
- Neškova M., Sirocky M., Nikutta R., Ivezić Ž., Elitzur M., 2008, *ApJ*, 685, 160
- Nicastro F., Martocchia A., Matt G., 2003, *ApJL*, 589, L13
- Panessa F., Bassani L., 2002, *A&AP*, 394, 435
- Pappa A., Georgantopoulos I., Stewart G. C., Zezas A. L., 2001, *MNRAS*, 326, 995
- Patel H., Clements D. L., Rowan-Robinson M., Vaccari M., 2010, *ArXiv e-prints*
- Piccinotti G., Mushotzky R. F., Boldt E. A., Holt S. S., Marshall F. E., Serlemitsos P. J., Shafer R. A., 1982, *ApJ*, 253, 485
- Pier E. A., Krolik J. H., 1992, *ApJ*, 401, 99
- Ptak A., Serlemitsos P., Yaqoob T., Mushotzky R., 1999, *ApJS*, 120, 179
- Ramos Almeida C., Levenson N. A., Rodríguez Espinosa J. M., Alonso-Herrero A., Asensio Ramos A., Radomski J. T., Packham C., Fisher R. S., Telesco C. M., 2009, *ApJ*, 702, 1127
- Reynolds C. S., Fabian A. C., Makishima K., Fukazawa Y., Tamura T., 1994, *MNRAS*, 268, L55+
- Risaliti G., Maiolino R., Salvati M., 1999, *ApJ*, 522, 157
- Rush B., Malkan M. A., Spinoglio L., 1993, *ApJS*, 89, 1
- Sandage A., Tammann G. A., Yahil A., 1979, *ApJ*, 232, 352
- Schulz H., Komossa S., Berghofer T. W., Boer B., 1998, *A&A*, 330, 823
- Sekiguchi K., Wolstencroft R. D., 1993, *MNRAS*, 263, 349
- Shu X. W., Liu T., Wang J. X., 2010, *ApJ*, 722, 96
- Simpson C., 2005, *MNRAS*, 360, 565
- Spinoglio L., Malkan M. A., 1989, *ApJ*, 342, 83
- Spinoglio L., Malkan M. A., Rush B., Carrasco L., Recillas-Cruz E., 1995, *ApJ*, 453, 616
- Thean A., Pedlar A., Kukula M. J., Baum S. A., O’Dea C. P., 2001, *MNRAS*, 325, 737
- Tran H. D., 2001, *ApJL*, 554, L19
- Tran H. D., 2003, *ApJ*, 583, 632
- Tran H. D., Osterbrock D. E., Martel A., 1992, *AJ*, 104, 2072
- Treister E., Urry C. M., Virani S., 2009, *ApJ*, 696, 110
- Tueller J., Baumgartner W. H., Markwardt C. B., Skinner G. K., Mushotzky R. F. e. a., 2010, *ApJS*, 186, 378
- Tueller J., Mushotzky R. F., Barthelmy S., Cannizzo J. K., Gehrels N., Markwardt C. B., Skinner G. K., Winter L. M., 2008, *ApJ*, 681, 113
- Turner T. J., George I. M., Nandra K., Mushotzky R. F., 1997, *ApJS*, 113, 23
- Ueda Y., Akiyama M., Ohta K., Miyaji T., 2003, *ApJ*, 598, 886
- Urry C. M., Padovani P., 1995, *PASP*, 107, 803
- Vaceli M. S., Viegas S. M., Gruenwald R., de Souza R. E., 1997, *AJ*, 114, 1345
- Vasudevan R. V., Fabian A. C., 2007, *MNRAS*, 381, 1235
- Veilleux S., Osterbrock D. E., 1987, *ApJS*, 63, 295
- Veron-Cetty M.-P., Veron P., 1986, *A&AS*, 66, 335
- Véron-Cetty M.-P., Véron P., 2006, *A&A*, 455, 773
- Wilkes B. J., Schmidt G. D., Cutri R. M., Ghosh H., Hines D. C., Nelson B., Smith P. S., 2002, *ApJL*, 564, L65
- Wills B. J., Wills D., Evans II N. J., Natta A., Thompson K. L., Breger M., Sitko M. L., 1992, *ApJ*, 400, 96
- Winter L. M., Lewis K. T., Koss M., Veilleux S., Keeney B., Mushotzky R. F., 2010, *ApJ*, 710, 503
- Zhang W. M., Soria R., Zhang S. N., Swartz D. A., Liu J. F., 2009, *ApJ*, 699, 281

Table 1: Optical line ratio data compiled from the literature and nuclear activity classification based on the scheme of Kewley et al. (2006). Also included are the observed fluxes of the [O III] emission line, the Balmer decrement, and the derived absorption corrected [O III] fluxes. Column (1) Galaxy name; Column (2) the emission line flux ratio [O III]/H $\beta$ ; Column (3) the emission line flux ratio [O I]/H $\alpha$ ; Column (4) the emission line flux ratio [N II]/H $\alpha$ ; Column (5) the emission line flux ratio [S II]/H $\alpha$ ; Column (6) the observed flux of the [O III]  $\lambda$ 5007 line in  $10^{-16}$  erg s $^{-1}$ ; Column (7) the Balmer decrement H $\alpha$ /H $\beta$ ; Column (8) the flux of the [O III] line corrected for absorption using the Balmer decrement; Column (9) reference for the line ratio data: 1=Armus et al. (1989), 2=Baan et al. (1998), 3=Corbett et al. (2003), 4=de Grijp et al. (1992), 5=Goncalves et al. (1999), 6=Ho et al. (1997), 7=Kewley et al. (2001), 8=Kim et al. (1995), 9=Kong et al. (2002), 10=Kopylov et al. (1974), 11=Maia et al. (1987), 12=Rodriguez, et al. In prep, 13=Seguchi & Wolstencroft (1993), 14=Vaceli et al. (1997), 15=Veron-Cetty & Veron (1986), 16=SDSS; Column (10) the activity classification based on diagram 1; Column (11) the activity classification based on diagram 2; Column (12) the activity classification based on diagram 3; Column (13) the adopted activity classification.

Name	[O III]/H $\beta$	[O I]/H $\alpha$	[N II]/H $\alpha$	[S II]/H $\alpha$	F <sub>[O III]</sub> (obs)	H $\alpha$ /H $\beta$	F <sub>[O III]</sub> (cor)	ref	1	2	3	classification	adopted
(1)	(2)	(3)	(4)	(5)	(6)	(7)	(8)	(9)	(10)	(11)	(12)	(13)	
MRK 0335	0.25	-	-	-	2250	-	-	12	-	-	-	Sy1.2	
NGC 0017	2.86	0.11	1.20	0.52	91	20.6	23800	12	AGN	Sy2	Sy2	Sy2	
NGC 0150	1.32	0.03	0.55	0.27	-	-	-	7	HII/AGN	HII	HII	HII	AGN
NGC 0214	-	-	-	-	-	-	-	-	-	-	-	Sy2	
NGC 0262	9.17	0.26	0.95	-	5170	3.2	5470	12	AGN	-	Sy2	Sy2	
UGC 00545	0.24	-	0.15	-	743	2.4	743	12	HII	-	-	Sy1	
NGC 0424	4.55	0.06	0.30	0.16	7000	2.9	7000	14	AGN	HII	Sy2	Sy2	
NGC 0526A	11.52	0.25	0.71	0.56	2470	3.0	2470	12	AGN	Sy2	Sy2	Sy1.5	
NGC 0513	3.05	0.11	0.75	0.46	490	3.1	490	12	AGN	Sy2	Sy2	Sy2	
NGC 0520	0.74	0.01	0.39	0.29	41	4.2	126	6	HII	HII	HII	HII	
NGC 0660	2.53	0.05	0.85	0.43	84	14.3	7520	6	AGN	Sy2	Sy2	Sy2	
2MASX J01500266-	5.25	-	0.55	-	535	7.5	7190	12	AGN	-	-	Sy2/LINER	
NGC 0695	0.30	0.05	0.45	0.17	-	7.7	-	8	HII	HII	HII	HII	
NGC 1052	2.00	0.92	1.12	2.22	2110	2.9	2110	12	AGN	LINER	LINER	LINER	
MESSIER 077	9.13	0.07	1.88	0.36	163000	4.3	438000	12	AGN	Sy2	Sy2	Sy2	
ARP 118	12.57	0.12	1.45	0.63	465	6.5	4160	12	AGN	Sy2	Sy2	Sy2	
MCG -02-08-039	18.14	0.18	0.53	0.27	1730	6.9	18100	12	AGN	Sy2	Sy2	Sy2	
NGC 1194	23.77	0.09	0.49	0.56	229	16.5	31400	16	AGN	Sy2	Sy2	Sy2	
NGC 1291	-	-	-	-	219	-	-	-	-	-	-	-	
NGC 1313	-	-	-	-	-	-	-	-	-	-	-	-	
NGC 1316	-	-	-	-	210	-	-	-	-	-	-	-	
NGC 1320	10.49	0.12	0.71	0.43	1240	5.6	6860	12	AGN	Sy2	Sy2	Sy2	
NGC 1365	1.83	0.04	0.48	0.16	620	8.8	13100	15	HII/AGN	HII	HII	Sy1.8	
NGC 1386	16.67	0.24	1.94	0.82	7800	2.8	7800	14	AGN	Sy2	Sy2	Sy2	
NGC 1482	0.21	-	0.42	0.29	-	-	-	7	HII	HII	-	HII	
3C 120	1.26	0.01	0.05	-	3820	6.9	39600	12	HII	-	HII	Sy1	
NGC 1614	1.05	0.03	0.57	0.22	912	11.1	38900	12	HII/AGN	HII	HII	HII/AGN	
MRK 0618	19.50	0.07	0.71	0.41	1410	-	-	7,12	AGN	Sy2	Sy2	Sy1	
NGC 1672	0.39	-	0.47	0.24	998	6.8	12600	12	HII	HII	-	HII	

NGC 1667	5.82	0.13	0.99	0.52	603	10.3	20600	12	AGN	Sy2	Sy2	Sy2
NGC 1808	0.16	0.02	0.54	0.21	145	14.2	16200	7,12	HII	HII	HII	HII
ESO 362- G 018	1.79	0.05	0.13	0.04	3650	4.0	7660	12	HII	HII	HII	Sy1.5
2MASX J05210136-	36.85	0.12	1.69	0.32	799	14.5	74200	12	AGN	Sy2	Sy2	Sy2
2MASX J05580206-	0.52	-	-	-	701	9.1	16400	12	-	-	-	Sy1
IC 0450	2.12	-	0.10	-	7000	7.6	97000	4	HII	-	-	Sy1.5
UGC 03973	1.23	0.02	0.12	0.11	14	6.4	120	16	HII	HII	HII	Sy1.2
IRASF07599+6508	0.30	-	-	-	33	33.6	36500	12	-	-	-	Sy1
NGC 2639	3.37	0.39	3.62	1.77	234	4.3	596	12	AGN	LINER	LINER	Sy1.9
NGC 2655	3.83	1.04	2.91	1.93	391	5.0	1590	6	AGN	LINER	LINER	LINER
IC 2431	0.61	0.03	0.36	0.30	62	4.7	263	16	HII	HII	HII	HII
MRK 0704	0.49	-	-	-	1410	7.9	22200	12	-	-	-	Sy1.5
NGC 2841	1.85	0.17	1.84	1.13	109	3.3	130	12	AGN	LINER	LINER	LINER
UGC 05101	2.29	0.08	1.27	0.40	45	19.7	10300	12	AGN	Sy2	Sy2	Sy2
NGC 2992	10.85	0.16	0.84	0.59	2930	7.3	36300	12	AGN	Sy2	Sy2	Sy1.9
MESSIER 081	1.14	0.21	0.37	0.23	2260	5.8	13900	12	HII/AGN	LINER	LINER	Sy1.8
MESSIER 082	0.36	0.01	0.56	0.18	316	25.0	146000	6	HII/AGN	HII	HII	HII/AGN
NGC 3079	3.60	0.18	1.59	0.86	18	23.6	7030	12	AGN	LINER	Sy2	Sy2
NGC 3147	6.14	0.15	2.71	1.14	172	5.3	828	12	AGN	LINER	Sy2	Sy2
NGC 3227	2.71	0.08	0.43	0.22	6180	6.3	50400	12	HII/AGN	HII	Sy2	Sy1.5
NGC 3310	0.95	0.04	0.66	0.26	340	4.8	1200	6	HII/AGN	HII	HII	HII/AGN
NGC 3486	4.52	0.09	1.04	0.93	131	3.3	159	12	AGN	LINER	Sy2	Sy2
NGC 3516	0.42	-	0.06	-	3630	3.0	3630	12	HII	-	-	Sy1.5
MESSIER 066	2.89	0.13	1.44	0.74	295	5.9	1960	12	AGN	LINER	Sy2	Sy2
NGC 3690	1.37	0.03	0.40	0.25	492	5.9	3230	6	HII/AGN	HII	HII	HII/AGN
NGC 3735	7.06	0.05	0.85	0.38	374	6.3	2940	12	AGN	Sy2	Sy2	Sy2
NGC 3976	3.50	0.10	1.95	0.83	77	4.4	210	12	AGN	LINER	Sy2	Sy2
NGC 3982	14.54	0.42	0.99	0.64	1810	3.5	2480	12	AGN	Sy2	Sy2	Sy2
NGC 4013	0.71	0.11	1.13	0.83	7	2.0	7	6	AGN	LINER	LINER	LINER
ARP 244	0.26	0.04	0.44	0.23	65	4.5	251	15	HII	HII	HII	HII
NGC 4051	1.59	-	0.26	0.14	3950	3.2	4490	12	HII	HII	-	Sy1.5
NGC 4151	2.51	-	0.16	-	126000	2.8	126000	12	HII	-	-	Sy1.5
NGC 4214	3.67	0.01	0.07	0.13	3470	2.8	3470	6	HII	HII	HII	HII
NGC 4253	1.68	-	0.23	-	4540	5.0	18900	4	HII	-	-	Sy1.5
MESSIER 099	0.90	0.02	0.48	0.23	29	6.3	226	6	HII/AGN	HII	HII	HII/AGN
MESSIER 100	0.79	0.11	1.18	0.48	52	4.6	160	6	HII	HII	LINER	LINER
NGC 4388	12.04	6.99	0.43	0.27	4890	4.8	17600	12	AGN	Sy2	LINER	LINER
NGC 4414	0.58	0.14	0.59	0.50	19	3.0	19	6	HII/AGN	HII	LINER	HII/LINER
NGC 4449	2.41	0.02	0.14	0.23	1780	3.2	2570	6	HII	HII	HII	HII
3C 273	-	-	-	-	-	-	-	12	-	-	-	Sy1
NGC 4490	2.55	0.12	0.25	0.71	33	6.3	262	6	HII/AGN	LINER	Sy2	HII/AGN
MESSIER 088	5.31	0.19	2.10	0.94	369	3.6	559	6	AGN	Sy2	Sy2	Sy2
NGC 4559	0.35	0.03	0.42	0.40	9	3.7	19	6	HII	HII	HII	HII
MESSIER 090	1.18	0.06	0.90	0.40	552	5.0	2250	6	AGN	HII	HII	HII/AGN
MESSIER 058	2.87	0.50	2.07	1.69	724	3.4	941	12	AGN	LINER	LINER	LINER
NGC 4593	22.91	0.12	1.26	0.29	1630	5.8	10400	7,12	AGN	Sy2	Sy2	Sy1

MESSIER 104	1.57	0.18	2.19	1.07	22	3.3	27	6	AGN	LINER	LINER	LINER
NGC 4631	1.53	0.03	0.24	0.23	23	3.0	28	6	HII	HII	HII	HII
NGC 4666	1.31	0.06	1.30	0.64	-	7.7	-	8	AGN	LINER	HII	HII/LINER
NGC 4725	-	-	-	-	-	-	-	-	-	-	-	Sy1
UGC 08058	0.37	-	-	-	1650	-	-	12	-	-	-	Sy2
NGC 4968	20.88	0.21	1.15	0.60	1340	9.6	37000	12	AGN	Sy2	LINER	LINER
NGC 5005	2.27	0.65	4.94	3.31	473	2.6	473	6	AGN	LINER	-	LINER
MESSIER 063	1.89	-	1.48	0.75	44	5.6	243	6	AGN	LINER	-	Sy2
MCG -03-34-064	11.72	0.22	1.29	0.46	15300	3.4	19600	12	AGN	Sy2	-	Sy2
NGC 5170	-	-	-	-	-	-	-	-	-	-	-	Sy2
NGC 5194	12.64	0.15	2.72	0.89	1630	8.9	36000	12	AGN	Sy2	-	Sy1.2
ESO 383- G 035	0.71	-	0.18	-	753	7.3	9150	4	HII	-	-	HII
MESSIER 083	0.29	0.02	0.44	0.21	336	6.1	3070	15	HII	HII	-	Sy1
IRAS F13349+2438	0.40	-	-	-	688	14.3	61900	12	-	-	-	Sy2
NGC 5256 (S)	2.65	0.13	0.76	0.55	322	-	-	12	AGN	Sy2	-	HII/AGN
NGC 5253	4.17	0.03	0.09	0.15	68000	2.9	68000	14	HII	Sy2	-	Sy2
MRK 0273	5.87	0.13	1.04	0.62	1800	9.2	44300	12	AGN	Sy2	-	Sy2
IC 4329A	0.64	0.01	-	0.02	2550	11.8	129000	12	-	HII	-	Sy1.2
UGC 08850 (E)	8.30	-0.02	0.40	0.45	7570	-	-	12	AGN	Sy2	-	Sy2
NGC 5506	8.59	0.12	0.67	0.53	4370	8.9	98400	12	AGN	Sy2	-	Sy2
NGC 5548	10.09	0.36	0.88	0.66	7340	1.3	7340	6	AGN	Sy2	-	Sy1.5
NGC 5775	18.41	0.10	0.75	0.65	6	125.9	332000	16	AGN	Sy2	-	Sy2
2MASX J15115979-	1.27	-	0.09	0.06	1910	8.6	38600	12	HII	-	-	Sy1
VV 705	0.92	0.03	0.50	0.27	118	7.9	1850	16	HII/AGN	HII	-	HII/AGN
UGC 09944	9.54	0.15	0.99	0.22	1460	6.1	10500	12	AGN	Sy2	-	Sy2
2MASX J15504152-	17.92	0.08	0.57	0.22	1600	7.2	18600	12	AGN	Sy2	-	Sy2
NGC 6240	1.43	0.31	1.26	1.24	76	16.0	9540	12	AGN	LINER	-	LINER
NGC 6286	0.45	0.08	0.49	0.33	-	-	-	2	HII/AGN	HII	-	HII/AGN
NGC 6552	-	-	-	-	-	-	-	-	-	-	-	-
AM 1925-724	5.25	0.14	1.15	0.72	-	-	-	7	AGN	Sy2	-	Sy1
NGC 6810	0.60	-	0.62	0.30	65	12.7	4100	12	HII/AGN	HII	-	HII/AGN
NGC 6890	33.33	0.16	1.25	0.43	980	13.3	71400	15	AGN	Sy2	-	Sy2
MRK 0509	0.40	-	0.18	-	5400	4.0	11100	4	HII	-	-	Sy1.2
ESO 286-IG 019	0.68	0.06	0.44	0.47	-	-	-	7	HII/AGN	HII	-	HII/AGN
NGC 7090	-	-	-	-	-	6.7	-	-	-	-	-	-
NGC 7172	4.77	0.10	0.99	0.45	40	3.5	57	12	AGN	Sy2	-	Sy2
NGC 7213	1.04	0.16	0.14	0.11	2380	7.9	37300	12	HII	LINER	-	HII/LINER
IC 5169	1.58	0.03	0.68	0.28	100	-	-	7,12	HII/AGN	HII	-	HII/AGN
NGC 7252	-	-	-	-	-	-	-	-	-	-	-	-
3C 445	2.89	0.02	-	0.04	2520	7.7	37100	12	-	HII	-	Sy1
NGC 7314	1.27	0.01	0.08	0.05	479	4.8	1700	12	HII	HII	-	Sy1.9
MCG -03-58-007	7.91	-	1.02	-	1270	3.8	2390	12	AGN	-	-	Sy2/LINER
NGC 7469	0.44	-	-	-	4540	-	-	12	-	-	-	Sy1.2
NGC 7479	3.97	0.22	1.20	1.01	140	4.9	533	12	AGN	LINER	-	Sy2
ESO 148-IG 002	2.69	0.04	0.20	0.22	282	9.7	8090	12	HII	Sy2	-	HII/AGN
NGC 7552	0.14	0.01	0.58	0.23	-	-	-	7	HII	HII	-	HII

NGC 7582	2.99	0.04	0.69	0.31	4530	7.0	49000	12	AGN	Sy2	Sy2	Sy2
NGC 7674	10.55	0.18	0.92	0.53	4780	3.4	6210	12	AGN	Sy2	Sy2	Sy2
NGC 7714	1.35	0.01	0.35	0.15	-	-	-	7	HII/AGN	HII	HII	HII/AGN
NGC 7771	1.04	0.04	0.48	0.41	-	-	-	8	HII/AGN	HII	HII	HII/AGN
MRK 0331	0.39	0.03	0.54	0.27	84	8.3	1540	12	HII/AGN	HII	HII	HII/AGN

Table 2: This table presents multi-wavelength data for our sample, which has been in the analysis in this chapter. Column (1) Galaxy name; Column (2) Optical type as determined in Table 1; Column (3) Broad line region information taken from Véron-Cetty & Véron (2006). h: hidden BLR detected in optical polarised light. i: broad lines detected in the near-IR, b: broad lines detected in the optical spectrum of a LINER or H II region; Column (4) Logarithm of the observed 2-10 keV luminosity ( $\text{erg s}^{-1}$ ); Column (5) Logarithm of the 12  $\mu\text{m}$  luminosity ( $\text{erg s}^{-1}$ ); Column (6) Logarithm of the absorption corrected [O III] luminosity ( $\text{erg s}^{-1}$ ); Column (7)  $\log_{10} N_{\text{H}}$  measured,  $\text{cm}^{-2}$ ; Column (8)  $\log_{10}(T=F_{2-10}/F_{\text{[OIII]}})$  where  $F_{2-10}$  is the observed X-ray flux, and  $F_{\text{[OIII]}}$  is the absorption corrected [O III] flux.

Name (1)	Type (2)	BLR (3)	$L_X$ (4)	$L_{12\mu\text{m}}$ (5)	$L_{\text{[OIII]}}$ (6)	$N_{\text{H}}$ (7)	T (8)
MRK0335	Sy1.2		43.45	44.01	-	20.56	-
NGC0017	Sy2		41.98	43.94	42.32	23.67	-0.93
NGC0150	HII/AGN		40.37	43.00	-	20.18	-
NGC0214			41.19	43.74	-	23.24	-
NGC0262	Sy2	h	43.34	43.79	41.44	23.12	1.71
UGC00545	Sy1		43.65	45.02	41.82	20.68	1.82
NGC0424	Sy2	h	42.52	43.98	41.34	23.37	0.29
NGC0526A	Sy1.5		43.29	43.68	41.31	22.06	1.96
NGC0513	Sy2	h	42.66	43.73	40.62	22.83	1.92
NGC0520	HII		39.95	43.40	39.21	20.49	0.68
NGC0660	Sy2		39.41	43.00	40.11	21.42	-0.70
2MASXJ01500266	Sy2/LINER	h	41.74	43.75	41.71	21.32	0.04
NGC0695	HII		41.62	44.52	-	20.84	-
NGC1052	LINER	h	41.49	42.48	40.07	23.49	1.34
MESSIER077	Sy2	h	42.15	44.51	42.14	24.18	-0.95
ARP118	Sy2		43.61	44.09	41.90	23.81	0.90
MCG-02-08-039	Sy2	h	42.93	44.25	42.57	23.67	-0.34
NGC1194	Sy2		42.32	43.46	42.11	23.83	-0.49
NGC1291			39.65	42.23	-	20.20	-
NGC1313			39.32	42.13	-	21.18	-
NGC1316			40.33	42.97	-	20.38	-
NGC1320	Sy2		42.65	43.14	41.08	24.31	-0.16
NGC1365	Sy1.8		42.46	43.87	40.94	23.24	1.00
NGC1386	Sy2	i	40.88	42.38	40.16	24.18	-0.39
NGC1482	HII		40.74	43.57	-	22.94	-
3C120	Sy1		44.19	44.43	43.00	21.03	1.06
NGC1614	HII/AGN		41.17	44.32	42.34	21.28	-1.17
MRK0618	Sy1		43.44	44.49	-	20.68	-
NGC1672	HII		39.59	43.43	40.73	20.48	-1.15
NGC1667	Sy2		42.76	43.91	42.03	24.43	-1.31
NGC1808	HII		40.39	43.52	40.59	22.94	-0.20
ESO362-G018	Sy1.5		42.37	43.30	41.42	23.19	0.64
2MASXJ05210136	Sy2	h	44.17	44.88	43.50	22.82	-0.37
2MASXJ05580206	Sy1		44.07	44.63	42.64	20.59	1.41

IC0450	Sy1.5	43.06	43.72	42.89	22.46	0.11
UGC03973	Sy1.2	43.78	44.00	40.13	20.72	3.00
IRASF07599+6508	Sy1	42.08	45.69	44.34	20.62	-2.26
NGC2639	Sy1.9	40.14	43.22	40.21	20.48	-0.08
NGC2655	LINER	41.72	42.61	39.89	23.36	0.82
IC2431	HII	41.37	44.79	41.19	20.57	0.18
MRK0704	Sy1.5	43.39	44.31	42.64	22.21	0.66
NGC2841	LINER	39.19	42.34	38.10	20.15	1.09
UGC05101	Sy2	42.45	44.50	42.57	23.70	-0.76
NGC2992	Sy1.9	43.05	43.23	41.68	21.61	1.37
MESSIER081	Sy1.8	38.77	40.89	37.86	20.71	0.90
MESSIER082	HII/AGN	40.11	43.25	40.20	20.71	-0.08
NGC3079	Sy2	40.87	43.29	40.33	24.18	-0.32
NGC3147	Sy2	41.44	43.68	40.21	20.46	1.23
NGC3227	Sy1.5	41.57	42.90	41.23	22.90	0.24
NGC3310	HII/AGN	40.32	42.99	39.46	20.85	0.86
NGC3486	Sy2	39.93	42.28	38.27	20.28	0.80
NGC3516	Sy1.5	43.77	43.23	40.80	23.51	1.63
MESSIER066	Sy2	39.48	43.12	39.40	20.32	0.07
NGC3690	HII/AGN	41.30	44.39	40.89	20.78	0.41
NGC3735	Sy2	40.21	43.45	40.72	20.48	-0.51
NGC3976	Sy2	40.09	42.96	39.51	20.04	0.52
NGC3982	Sy2	40.16	42.55	39.87	23.34	-0.12
NGC4013	LINER	39.02	42.38	37.07	22.95	1.77
ARP244	HII	40.39	43.55	39.26	20.51	1.12
NGC4051	Sy1.5	40.91	42.60	39.72	23.27	1.07
NGC4151	Sy1.5	42.09	43.07	41.48	22.78	0.57
NGC4214	HII	38.95	42.21	39.37	20.78	-0.43
NGC4253	Sy1.5	42.96	43.51	41.85	20.26	1.11
MESSIER099	HII/AGN	40.00	44.12	39.51	20.46	0.49
MESSIER100	LINER	40.06	43.59	38.98	20.30	1.07
NGC4388	LINER	42.89	43.61	41.44	23.60	1.08
NGC4414	HII/LINER	39.33	42.98	37.38	20.20	1.95
NGC4449	HII	38.51	41.57	38.44	20.30	0.05
3C273	Sy1	45.82	46.15	-	20.26	-
NGC4490	HII/AGN	39.49	42.57	38.32	21.30	1.16
MESSIER088	Sy2	41.69	43.87	39.86	24.18	0.33
NGC4559	HII	39.91	42.29	37.49	21.04	2.41
MESSIER090	HII/AGN	37.25	40.52	37.60	20.45	-0.35
MESSIER058	LINER	41.35	43.23	39.73	20.45	1.62
NGC4593	Sy1	42.84	43.33	41.27	20.30	1.56
MESSIER104	LINER	38.89	41.10	36.18	20.85	2.71
NGC4631	HII	38.90	43.08	37.39	21.32	1.51
NGC4666	HII/LINER	40.48	43.71	-	20.23	-
NGC4725		39.25	42.31	-	19.95	-
UGC08058	Sy1	42.47	44.70	-	22.85	-

i

h

b

NGC4968	Sy2		43.22	43.53	41.91	24.48	-1.15
NGC5005	LINER	b	39.91	42.97	39.03	20.04	0.88
MESSIER063	LINER		39.17	42.95	38.19	20.60	0.94
MCG-03-34-064	Sy2	h	42.95	44.16	42.08	23.60	0.12
NGC5170			39.34	42.74	-	21.18	-
NGC5194	Sy2		40.43	43.13	40.25	24.18	-0.93
ESO383-G035	Sy1.2		42.75	43.04	41.08	20.59	1.64
MESSIER083	HII		39.41	43.62	39.29	20.60	0.11
IRASF13349+2438	Sy1		43.81	45.66	44.26	22.02	-0.46
NGC5256	Sy2		42.21	44.13	-	23.24	-
NGC5253	HII/AGN		37.94	41.66	40.47	20.60	-2.53
MRK0273	Sy2		42.84	44.26	43.17	23.78	-1.08
IC4329A	Sy1.2		43.75	44.21	42.88	20.66	0.87
UGC08850	Sy2	h	43.15	44.85	-	23.59	-
NGC5506	Sy2	i	42.85	43.43	41.92	22.51	0.84
NGC5548	Sy1.5		43.43	43.86	41.69	20.20	1.74
NGC5775	Sy2		39.84	43.50	42.36	21.72	-2.74
2MASX-J15115979	Sy1		43.94	44.54	43.26	20.92	0.35
VV705	HII/AGN		42.35	44.47	41.84	23.93	-0.19
UGC09944	Sy2		41.60	44.04	42.16	20.45	-1.32
2MASX-J15504152	Sy2	h	43.00	44.10	42.59	24.18	-0.62
NGC6240	LINER		43.49	44.34	42.12	24.05	0.30
NGC6286	HII/AGN		40.58	43.96	-	20.26	-
NGC6552		h	42.88	43.95	-	24.18	-
AM1925-724	Sy1		42.79	44.77	-	23.58	-
NGC6810	HII/AGN		39.91	43.53	40.62	20.70	-0.71
NGC6890	Sy2		42.18	43.12	42.02	24.18	-1.41
MRK0509	Sy1.2		44.00	44.31	42.48	20.62	1.52
ESO286-IG019	HII/AGN		42.31	44.55	-	23.69	-
NGC7090			39.82	42.27	-	21.15	-
NGC7172	Sy2		42.74	43.26	38.98	22.93	3.57
NGC7213	HII/LINER	b	42.66	43.08	41.44	20.04	0.77
IC5169	HII/AGN		40.72	43.20	-	20.04	-
NGC7252			40.36	43.69	-	20.30	-
3C445	Sy1		43.94	44.94	43.45	23.54	0.27
NGC7314	Sy1.9	h	42.33	42.85	39.94	21.78	2.37
MCG-03-58-007	Sy2/LINER	h	42.74	44.11	41.69	23.44	0.58
NGC7469	Sy1.2		43.25	44.37	-	20.64	-
NGC7479	Sy2		42.04	43.69	39.87	24.30	0.79
ESO148-IG002	HII/AGN		43.21	44.59	42.58	24.18	-0.68
NGC7552	HII		40.21	43.79	-	20.11	-
NGC7582	Sy2	i	42.61	43.56	41.48	24.18	-0.34
NGC7674	Sy2	h	43.62	44.49	42.08	24.18	-0.01
NGC7714	HII/AGN		40.52	43.27	-	21.15	-
NGC7771	HII/AGN		40.92	44.05	-	20.70	-

MRK0331	HII/AGN	40.67	43.95	41.08	21.08	-0.41
---------	---------	-------	-------	-------	-------	-------